Idiosyncratic neural coding and neuromodulation of olfactory individuality in *Drosophila*

Kyle Honegger[1,2,†], Matthew Smith[1,†], Matthew Churgin[1], Glenn Turner[3], Benjamin de Bivort[1*]

1 — Department of Organismic and Evolutionary Biology & Center for Brain Science, Harvard University, Cambridge, MA 02138

2 — Ann & Robert H. Lurie Children's Hospital of Chicago, Chicago, IL 60611

3 — Janelia Research Campus, Howard Hughes Medical Institute, Ashburn, VA 20147

† — contributed equally

* — correspondence: debivort@oeb.harvard.edu

Keywords: odor preference, individuality, idiosyncratic behavior, sensory stimuli, neural encoding, circuit analysis, neuromodulation, serotonin, dopamine, nutrition

Abstract

Innate behavioral biases and preferences can vary significantly among individuals of the same genotype. Though individuality is a fundamental property of behavior, it is not currently understood how individual differences in brain structure and physiology give rise to idiosyncratic behaviors. Here we present evidence for idiosyncrasy in olfactory behavior and neural responses in *Drosophila*. We show that individual female *Drosophila* from a highly inbred lab strain exhibit idiosyncratic odor preferences that persist for days. We used *in vivo* calcium imaging of neural responses to directly compare projection neuron (second-order neurons that convey odor information from the sensory periphery to the central brain) responses to the same odors across animals. We found that, while odor responses appear grossly stereotyped, upon closer inspection, many individual differences are apparent across

antennal lobe (AL) glomeruli (compact microcircuits corresponding to different odor channels). Moreover, we show that neuromodulation, environmental stress in the form of altered nutrition, and the activity of certain AL local interneurons affect the magnitude of inter-fly behavioral variability. Taken together, this work demonstrates that individual *Drosophila* exhibit idiosyncratic olfactory preferences and idiosyncratic neural responses to odors, and that behavioral idiosyncrasies are subject to neuromodulation and regulation by neurons in the antennal lobe.

Introduction

Olfaction is a deeply personal sense. We know from common experience that smells elicit strong reactions linked to both past experiences and the perceptual qualities of the odors themselves. Behavioral reactions to an odor (e.g., durian or gasoline) can vary greatly from individual to individual, in some cases evoking responses that range from attraction to utter aversion, but the mechanisms by which volatile molecules are mapped into perceptual space [1-3] and drive behavior are currently not well understood. In humans, both socio-cultural experience [4-6] and genetic polymorphisms in odorant receptors [7,8] have been shown to explain some of the individual variation in odor perception. In a particularly clear example, people with hypomorphic receptor mutations experience specific anosmias for cognate odors [9]. Presumably, such alterations in sensory detection affect downstream neural responses, and thus odor perception, but currently relatively little is actually known about how this idiosyncrasy manifests in the activity of deeper neural circuits.

A major obstacle to studying idiosyncrasy in neural circuit responses to stimuli has been the need to identify corresponding circuit elements across individuals. This is difficult to do in large organisms with complex, redundant neural circuits, where individual neurons are not identifiable (i.e., directly comparable) across individuals. Moreover, testing hypotheses about the involvement of specific circuit components in shaping the distribution of behavioral responses across individuals requires large sample sizes (often hundreds of individuals, because precisely measuring a distribution requires measuring rare individuals in its tails). This requirement alone largely precludes the use of mammals, or other large vertebrates, to study these effects.

We addressed these challenges by leveraging the identifiable and grossly stereotyped neuroanatomy of the antennal lobe (AL) of the fruit fly, *Drosophila melanogaster*. The *Drosophila* AL has around 50 identifiable odor-coding channels, which are conveniently arranged into spatially discrete glomeruli

[10-12]. The glomeruli display remarkable stereotypy in their source of sensory neuron inputs, anatomical position, relative sizes, and efferent innervation by extrinsic projection neurons (PNs) that convey odor information to deeper areas of the brain [13-15]. Overlaid on this coarse stereotypy, however, is a complex network of dense inter-glomerular connections provided by a population of physiologically diverse AL local neurons (LNs) [16,17]. The roles played by these LNs in shaping and modulating AL odor responses are diverse [16-19] and may offer several mechanisms for diversifying odor responses in the AL. In one study of the morphology of single LNs, there were far more anatomical classes of LNs across individuals than there are LNs per hemisphere in an individual fly [16]. So it must be the case that the complement of LN wiring configurations in each fly is unique to that individual.

Individuality in *Drosophila* behavior has been observed in phototaxis [20], spontaneous locomotor biases [21], thermal preference [22], spontaneous microbehaviors [23,24], and object-fixated locomotion [25]. These differences are persistent over days and represent something like fly personality. Individual behavioral outcomes likely have a partial origin in stochastic events during development [26], and genetic factors determine the magnitude of behavioral variability in isogenic populations [27]. At the same time, the acute, post-developmental activity of specific neural circuits also tunes individuality, meaning it is potentially under the real-time control of the nervous system [20,21]. It is likely that these factors are at work in regulating individual odor preferences, but the extent of individuality of odor coding — whether individual nervous systems represent the same stimulus in the same way — has not been examined in this context. Using an automated odor-preference assay, we measured significant individuality in odor preference that was stable across days. Using volumetric two-photon microscopy, we observed individuality in the representation of odors in the antennal lobe. Pharmacological and thermogenetic experiments established that multiple neuronal subtypes in the antenna lobe and neuromodulatory axes affect odor preference individuality, forming a circuit with the potential to dynamically tune odor preference variability in response to environmental cues.

Results

To determine whether individual flies exhibit idiosyncratic odor behaviors, we built an instrument to measure the odor preference of 15 individual flies simultaneously (Figure 1A). In this rig, each fly moves freely through a linear corridor in which two odor stimuli are pumped [28]. The airflow bearing these odor cues is laminar, forming a sharp boundary between the two odor compartments at the

middle of the corridor (Figure 1B and S1A). The position and orientation of each animal was tracked automatically with machine vision. Each experiment consisted of a three minute “pre-odor period” in which clean air was pumped into both compartments followed by a three minute “odor-choice period” when alternative odor stimuli filled each half of each arena, lastly followed by a 30 second “post-odor period” of clean air (Figure 1C).

In this setup, flies expressed olfactory preference by walking into, and staying in their preferred odor compartment (Figure 1C). Preference was quantified as the fraction of time each fly spent in a compartment. For example, in experiments where flies chose between odorants 3-octanol (OCT) and 4-methylcyclohexanol (MCH), preference was quantified as the proportion of time in OCT (with 0/1 indicating a complete preference for MCH/OCT respectively). In a clear sign that flies express odor preference in this assay, we observed that they frequently turned around at the compartment boundary (Figure S1B) when odors were present, while far fewer reversals occurred in the absence of odor (Figure 1C). The frequency of these reversals decreased over the course of the three minute odor-choice period, presumably as flies adapt/habituate to the stimuli. Thus, the odor-choice period and our quantification of preference were limited to three minutes.

We observed a broad distribution of odor preference scores in OCT-MCH choice experiments among highly inbred wild type (iso^{KH11} strain; see Methods) females, reared in the same environment. Indeed, the observed distribution was broader than we would expect to observe under a null model in which all animals sample their odor-choice behavior from the same distribution (Figure 1D; $p < 0.001$). Even in such “all flies are identical” scenarios, one would still observe apparent variation in the measured preference scores because we are only able to assess odor choices over a three minute window. That the observed distribution is broader than this null distribution (dashed lines in Figure 1D, F) indicates that flies are behaving idiosyncratically. Additionally, the observed distribution of preference scores was broader than the distribution of “sham” scores calculated from the pre-odor period (i.e., arbitrarily assigning one half of the un-odorized arena to be OCT for purposes of calculating a preference index; gray lines in Figure 1D), whose dispersion reflects individual variability in locomotion and sampling error (Figure S1C, D) but not responses to odors. We quantified this difference in variance between the observed and null behavioral distributions as an “Individuality score,” which, at 0.0174 for the OCT-MCH choice, was significantly greater than 0 ($p < 0.001$; See Methods). Beyond the pair of aversive odorants OCT and MCH, we also observed idiosyncratic odor preferences in experiments in which flies chose between clean air and odorants 3-octanol (Figure 1F, left; Individuality score = 0.0047, $p < 0.001$), 1-butanol (Figure 1F, middle; Individuality score = 0.012, $p < 0.001$), and 2-heptanone (Figure 1F, right; Individuality score = 0.015, $p < 0.001$). Importantly, we also confirmed that

idiosyncratic preferences persist across days (Figure 1G), as observed for other idiosyncratic fly behaviors [20-22,27].

Idiosyncratic behavior presumably has a basis in idiosyncratic patterns of odor-induced neural activity. We hypothesized that such response idiosyncrasies might be observable in the sensory periphery of the olfactory circuit, specifically in the glomeruli of the antennal lobe. To test this hypothesis, we built a stage for delivering the same odorant stimuli from our behavioral instrument to flies being imaged for Ca^{++} activity with a 2-photon microscope (Figure 2A). As with the behavioral instrument, odor stimuli in the imaging rig were computer-controllable and for each experiment we stimulated flies with three panels of odorant cues (Figure 2B). In the first two panels, 12 different monomolecular or purified extract odorants were delivered for 4 seconds each, with a ~80s pause between odors, in a random order. In the third panel, OCT and MCH were delivered in alternation up to 5x times each, with the same timing, and starting randomly with either OCT or MCH. For 24 seconds, starting 6 seconds prior to odor onset, we recorded fluorescence in the dendritic compartment of Projection Neurons (PNs; Figure 2C) using the transgenic line GH146 to drive expression of GCaMP6m in roughly two-thirds of all glomeruli. These recordings were volumetric, and scan volumes (85μm x 70μm x 12 z-planes spaced ~6.5 μm apart), covering all GH146-positive glomeruli, were acquired at ~0.8Hz.

As expected, we observed a variety of Ca++ responses in PN dendrites (Figure 2D, E and S2), including excitatory and inhibitory responses to both odor onset and odor offset. As expected, the exact responses depended on the glomerulus (Figure 2D) and the odor (Figure 2E). To characterize the population responses in PNs to each odor, we sought to systematically compare odor responses across many glomeruli. We developed a semi-automated pipeline for assigning glomerular labels to recording voxels. This pipeline used *k*-means clustering to identify sets of voxels with similar response dynamics, and priors about glomerular size and geometric configuration to provide a list of potential glomeruli, which was finally labeled with glomerular identities (Figure 2F-G) and pruned of any non-glomerular clusters manually. Given variation in transgenic expression, imaging preparation and mounting geometry, we were not able to identify every glomerulus in every animal. But, we were able to efficiently characterize the odor responses of dozens of animals, to a dozen odors, in 3 to 15 glomeruli, with a mean of 10 (Figure S2).

Immediately, we noticed that the responses of some glomeruli were very different across individuals, while appearing consistent across multiple presentations of the odorant within an individual (Figure 2F2-G2). To assess this systematically, we projected the multidimensional glomerulus-odor responses onto their first two principal components (Figure 2I; See S3 for eigenvalues and odor response

covariance), where we observed that within-fly responses (i.e., across presentations) were, on average, closer than between-fly responses ($p < 0.001$ by bootstrap resampling). This was also true when we examined the responses of OCT and MCH specifically in the space of responses to the OCT/MCH stimulus panel (Figure 2J,K; $p < 0.001$ and $p < 0.01$, respectively). Separately, we confirmed that this pattern was not an artifact of in-filling missing data for the PCA, as it was also observed in smaller data sets with no missing data (Figure S4). Thus, neural responses to odors appear to differ significantly across individuals, often qualitatively.

It has been previously shown that neuromodulators, specifically serotonin, affect the degree of idiosyncrasy in another stimulus-response behavior, phototaxis [20]. We tested whether neuromodulatory pathways also had an effect on individual odor preferences. We first examined the role of serotonin by feeding flies increasing doses of the serotonin synthesis inhibitor alpha-methyltryptophan (α-MW; 20 or 40mM; [29]). Flies fed α-MW appeared to show a dose-dependent reduction in variability compared to control flies. By contrast, feeding with the serotonin precursor 5-hydroxytryptophan (5-HTP; [29]) had little effect (Figure 3A). While dopamine pharmacological experiments had no effect on phototactic idiosyncrasy [14], the key role of dopamine in olfactory associative conditioning in the mushroom bodies [30,31], led us to hypothesize that dopamine could be essential to tuning individual odor preferences in an experience-dependent fashion (even in the absence of structured associative training). Flies bearing a mutant allele of the *Dop1R1* dopamine receptor gene (*Dop1R1*^{f02676}, hereafter referred to as *Dop1R1* flies [31,32]), also exhibited lower idiosyncrasy (narrower behavioral distributions) than control flies (Figure 3B). Conversely, flies fed the dopamine precursor L-DOPA [30,31] exhibited higher idiosyncrasy. The lower idiosyncrasy of *Dop1R1* could likely not be explained by anosmia, as these flies exhibited reversal behaviors at the odor boundary during the odor-choice period, though they may have habituated to odors faster than wild type flies (Figure S5).

In conducting these experiments, we realized that our experimental manipulations changed not only the apparent variability of behavior, but also its mean, and for our choice of odor preference metric, the mean and variance are coupled. We also suspected that seasonal effects, such as those that affect insect olfactory conditioning [33] might also affect our measured preferences and variabilities. Indeed, variability was higher in the winter — an effect that could be modeled as a linear function of Boston outdoor air temperatures (despite experimental flies being grown in temperature- and humidity-controlled incubators and tested in environmentally-controlled rooms; Figure S6B-E). Moreover, we had more confidence in our measure of some individuals' preferences than others — it is hard to characterize the preference of flies that don't walk much in the arenas.

We implemented a Bayesian linear modeling framework (Figure 3C) to estimate and control for each of these effects, disentangle the coupling of mean and variance, and assign more weight to inferences based on flies that were active and expressed preference more clearly. See Methods for details. The output of this analysis was posterior distributions for each parameter of the model (Figure S6), and we were particularly interested in the posterior distributions on the variance effects of genotype, experimental condition, and genotype-by-experimental condition parameters corresponding to our neuromodulatory manipulations (Figure 3D). Consistent with our observations of single experiments, we found that 5-HTP has no strong effect on variability, while α-MW had a substantial negative, dose-dependent effect (i.e., 0 was above the 95% credible interval for the α-MW effect parameters). Additionally, *Dop1R1* mutation reduced variability substantially, while L-DOPA increased it.

Serotonin neuromodulation appears to regulate behavioral idiosyncrasy, but does it also regulate idiosyncrasy in the neural responses to odors? We imaged PN dendrite (GH146>GCaMP6m) responses in flies that had been fed 40mM α-MW for three days and matched controls (raw data in Figure S7). We again observed that the distance between odor presentations in response space was less within a fly than between flies (Figure 3E-G). This was true in both control flies ($0.001 < p < 0.01$) and α-MW-treated flies ($0.01 < p < 0.05$). The distance between α-MW-treated and control odor responses both within and between flies was higher in α-MW-treated flies. These differences were not statistically significant ($p > 0.05$), though they were seen for all projections onto the first n principle components, as well as the first 4 PCs separately (Figure S4C,D). The inter-fly distances of α-MW-treated responses did appear to be significantly greater than control responses on PC4 ($p = 0.028$) as did the intra-fly distances ($p = 0.026$), though these analyses would not survive a test for multiple comparisons.

Next, we sought to examine the neural circuit basis of the modulatory effects on behavioral variability. We used thermogenetic effectors to activate or inhibit circuit elements within the olfactory system, and recorded the odor preferences of many individuals subject to this manipulation (Figure 4A,B). First we targeted the contralateral serotonin-immunoreactive deutocerebral neurons (CSD; [34]) using two independent Gal4 lines. These serotonin-positive neurons have post-synaptic compartments distributed widely across the olfactory system and project axons into the antennal lobe contralateral to their cell body. Again, applying a Bayesian framework to infer the effects of these thermogenetic manipulations (Figure 4D; S8), we found that activating CSD neurons with dTRPA1 (an effector that depolarizes neurons at high temperatures; [35]) had no effect on variability (Figure 4E).

While acutely activating CSD may not have an effect on variability, the antennal lobe local neurons (LNs) express multiple serotonin receptors [26], and are plausible candidate regulators of variability because they have highly variable morphology across individuals [16,36]. We found that activating and inhibiting different populations of LNs often had the effect of reducing behavioral variability. Specifically, the following thermogenetic genotypes had variance-reducing effects at the induced temperature: for each of the LN Gal4 lines: *R14H04>dTRPA1*, *R14H04>Shibire^{ts}* (probably), *R46E11>dTRPA1*, *VT046560>dTRPA1*, and *VT046560>shibire^{ts}*. (The shibire^{ts} effector silences neurons by blocking vesicular release at the restrictive temperature [37].) These Gal4 lines express in different subsets of LNs of varying count and, presumably, varying physiology, but normal neuronal activity in LNs appears to be required acutely for normal levels of behavioral variability. Lastly, we manipulated the activity of tachykinin-expressing (Tk+) neurons (using the R61H07 Gal4 line [38]), which overlap with a specific subset of LNs. We found that activating Tk+ cells with dTRPA1 probably increased variability, while silencing them had no effect. Thus, the effect of thermogenetically perturbing Tk+ cells appears to be inconsistent with the variability-reducing effect of perturbing LNs.

Neuromodulatory dynamics in the antennal lobe have been previously implicated in changing odor-induced responses in a state-dependent manner. Specifically, short neuropeptide F (sNPF) and tachykinin mediate starvation-dependent changes in glomerular responses which predict changes in behavioral valence [34]. We hypothesized that subjecting flies to environmental stress by switching them from our standard cornmeal/dextrose food to a reconstituted commercial mix might induce an increase in behavioral variability, potentially as a bet-hedging response (i.e., when the environment fluctuates, it may be adaptive to diversify stimulus responses, thereby increasing the chance that some individuals implement behaviors suitable to the new environment; [22]). We reared flies on freshly prepared cornmeal/dextrose food before giving them a “food shock” by switching them onto reconstituted commercial flake food (Formula 4-24 from Carolina Biological Supply) for one day. As controls, we switched them onto fresh rich food and, alternatively, fed them chronically (for three days) on flake food. These manipulations had significant effects on the mean preference in an OCT-MCH choice assay, but also showed higher variability in the food shock condition (Figure 5A). We used our modeling framework to disentangle (Figure 5B) these effects, and found that food shock increased variability substantially (Figure 5C). In contrast, flies chronically fed on F4-24 flake food since eclosion showed lower variability than controls. Feeding the flies α-MW partially blocked the effects of the food shock, reducing odor preference variability in the same direction as our earlier pharmacological experiments (Figure 3A,D).

Discussion

Odors evoke highly individualized perceptions in humans. We set out to study this in a genetic model system, where high throughput behavioral automation and circuit-mapping tools could be brought to bear. Using a custom-built, automated instrument in which flies walk freely in a linear chamber where each half can be filled independently with a unique odor cue, we observed that flies exhibit idiosyncratic odor preference behaviors (Figure 1). These individual preferences are evident in choices between two odorants and in choices between odors and air, and persist for days, representing something like odor-preference personality. Linear chambers with odorizable compartments have been previously used to study learning and memory, and the authors reported that odor responses appeared idiosyncratic [28], though other studies emphasized the consistency of individual responses [39]. A challenge with this approach was the limited window in which flies expressed an odor preference (roughly three minutes) before appearing to habituate [40] and ignore the odor boundary (Figure 1C). We tried various protocols to rapidly dishabituate flies to the odors, with no success. Ultimately, this meant that we could collect only a limited amount of data per fly. The modest day-to-day repeatability (r=0.35) compared to other measures of fly personality [20-22] was likely attributable to the amount of data we collected per fly. This constraint partly motivated our use of Bayesian modeling to assess the effects of our manipulations.

Despite the well-known anatomical and functional stereotypy in the peripheral olfactory system, we observed individuality in odor coding in the antennal lobe, the site of initial olfactory integration. The Ca^{++} responses of projection neurons (across glomeruli) were idiosyncratic and persistent when the same odor was presented to different flies (Figure 2). In some cases these differences were even sign-reversing: an odor would activate a glomerulus in one fly but inhibit it in another. Some of the observed individuality of coding may be due to artifacts of dissection, mounting or variable expression of the Ca++ indicator. Still, the observation of qualitatively different glomerular responses, which are consistent within the individual, is not easily attributable to such causes. Odor representations in the PNs are more broadly distributed in odor space than ORN representations [41], and the circuit dynamics that underlie this broadening may also contribute to distinguishing representations across individuals. Establishing the significance of observed physiological differences may ultimately come down to the ability to predict idiosyncratic behaviors from idiosyncratic coding, as this circuit may produce consistent outputs even with idiosyncratic internal states [42]. For now, we believe that the prevailing view that odor responses in the antennal lobe are highly stereotyped across individuals should be tempered.

Neuromodulatory axes have been previously implicated as affecting the amount of behavioral variability exhibited by isogenic animals; disrupting serotonin increased variability in fly phototaxis [20], while in *C. elegans* it decreased variability in locomotor activity [43]. Tyramine/octopamine had the opposite effect in worms, so multiple modulatory axes appear to regulate variability. Indeed, we observed that *Dop1R1* mutation strongly decreased odor preference variability (conversely, feeding flies L-DOPA increased variability; Figure 3). Inhibiting serotonin had a dose-dependent effect of decreasing variability in odor preference. The Bayesian framework we used to infer these effects also allowed us to estimate a surprising environmental effect. Odor preference variability was consistently higher in the winter (Figure S6), and this could be modeled as a linear function of the outdoor air temperature in Boston. This effect was large despite our rearing flies in temperature- and humidity-controlled incubators and measuring behavior in temperature- and humidity-controlled environmental rooms. We suspect that outdoor air temperature is only a correlate of the true seasonal cause of fluctuating variability, for which there are many possibilities including plant [44] or yeast [45] volatiles, or barometric pressure [46].

In flies chronically fed serotonin inhibitor, we observed that within-fly odor responses were more similar than between-fly responses (Figure 3E-G), as was seen in control flies (Figure 2I). The distances between odor responses were generally higher in α-MW-fed flies than controls, but these differences were not statistically significant except perhaps on the fourth principal component of response variation (Figure S4). Serotonin's effect on behavioral variability may reside outside the antennal lobe, or our imaging experiments may be underpowered to detect modulatory effects on odor coding. We found that acutely activating the serotonin-immunopositive CSD neurons had no effect on behavioral variability (Figure 4E), in contrast with the chronic pharmacological experiments, but consistent with reported effects on AL activity [47]. The apparent long timescale of serotonin effects on behavioral variability may reflect a role in regulating circuit structure, consistent with its role in neurodevelopment [36]. Many cell types in the AL express a diversity of serotonin receptors [26] and may be intermediary in the effect of serotonin pharmacological manipulation and behavioral variability. These include the LNs, which, when silenced or activated resulted in lower odor preference variability (Figure 4; and, presumably, a less sparse and regularized pattern of PN activity [48]). This suggests an endogenous role of increasing variability, consistent with their morphological variability across individuals [16]. These effects varied in magnitude by LN subpopulation, perhaps reflecting their physiological diversity. Indeed, LNs may have heterogeneous effects on variability that compete with each other across the AL to determine odor preference variability.

In addition to the variability-reducing effect of perturbing LNs, we identified two other manipulations that reduced variability: serotonin pharmacological manipulation and mutation of *Dop1R1*. These

experiments suggest that the endogenous role of these factors, with respect to odor preference, is to increase the variability across individuals. *Dop1R1* facilitates synaptic plasticity in the mushroom body in support of associative conditioning [31,49], but we found that thermogenetic manipulations of the mushroom body had no consistent effect on odor preference variability (Figure S8). So perhaps the effect of *Dop1R1* and L-DOPA is in another neuropil, such as the central complex, where it is known to modulate locomotion [50,51]. Indeed, the reversal behavior seen at the odor boundary may be supported by an idiothetic path-integration functionality thought to be implemented in the central complex [52-54].

In previous work, we found that genetic variants [27] and circuit manipulations [8,10] predominantly increased variability, as if we had disturbed mechanisms for suppressing variability. The results in this study suggest that there may be evolved mechanisms to increase variability, perhaps as part of a bet-hedging strategy [22,24]. Such a mechanism, under the control of the nervous system, could respond rapidly to environmental fluctuations to diversify the behavior of a population and allow individuals to exhibit behavioral phenotypes fit for the new environment. We tested this notion by subjecting flies to a rapid change in their food, from their normal cornmeal/dextrose food to a commercial flake food on which flies grow less successfully [55]. This food shock caused an increase in odor preference variability, but only over short timescales. After three days on the flake food, variability went back down. Feeding flies serotonin synthesis inhibitor during this food shock suppressed the increase in variability (Figure 5). Taken together, these findings suggest that odor preference variability is under the acute control of several specific neuron types in the AL, and possibly elsewhere, and over longer timescales by modulatory pathways that may also affect odor-coding idiosyncrasy. These axes of flexibility may facilitate bet-hedging strategies by which animals can respond to environmental fluctuations with adaptive changes in their behavioral diversity.

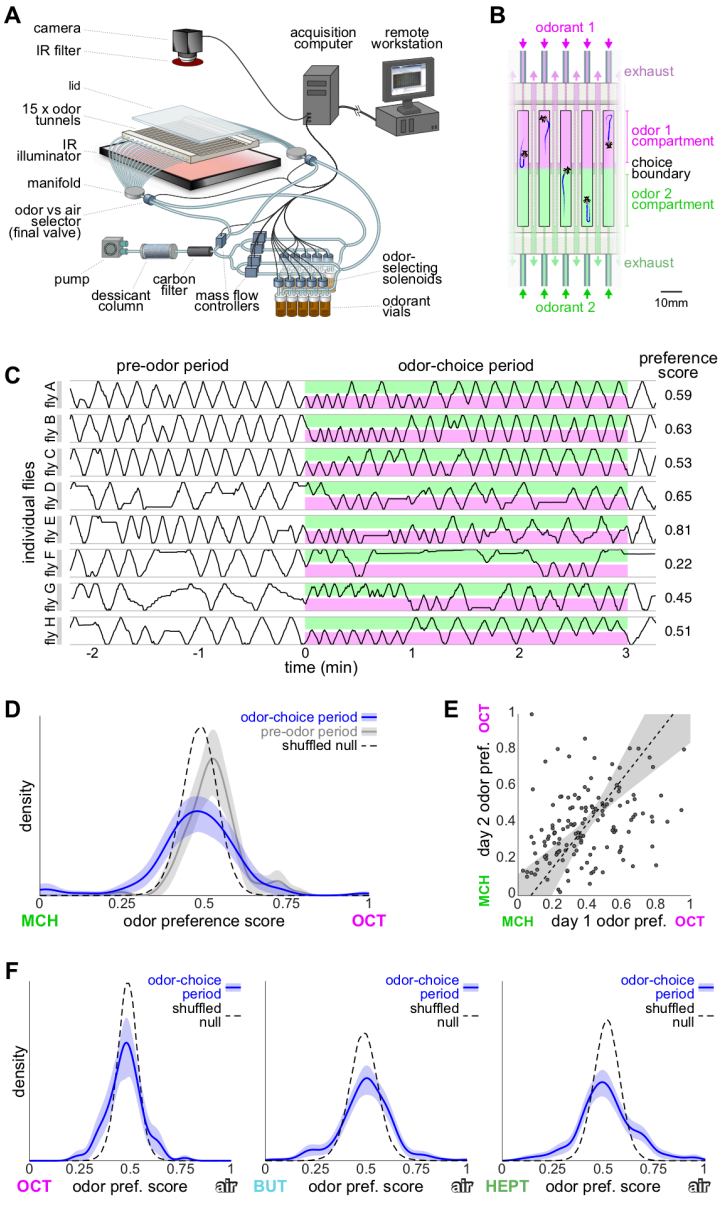
A
camera
IR filter
lid
15 x odor tunnels
IR illuminator
manifold
odor vs air selector (final valve)
pump
dessicant column
carbon filter
mass flow controllers
acquisition computer
remote workstation
odor-selecting solenoids
odorant vials
B
odorant 1
exhaust
odor 1 compartment
choice boundary
odor 2 compartment
exhaust
odorant 2
10mm
C
pre-odor period
odor-choice period
preference score
individual flies
fly A
fly B
fly C
fly D
fly E
fly F
fly G
fly H
0.59
0.63
0.53
0.65
0.81
0.22
0.45
0.51
-2
-1
0
1
2
3
time (min)
D
odor-choice period
pre-odor period
shuffled null
density
0
0.25
0.5
0.75
1
MCH
odor preference score
OCT
E
day 2 odor pref.
OCT
MCH
day 1 odor pref.
F
odor-choice period
shuffled null
density
OCT
odor pref. score
air
BUT
HEPT

Figure 1 - Individual flies have idiosyncratic odor preferences

A) Schematic of the odor-preference experimental apparatus. Briefly, air is drawn in from the room, cleaned and dehumidified, and pumped through the headspace of one of twelve odorant vials, with the vial selected using computer-controlled solenoid valves. Mass-flow controllers standardize the flow rate, and the odorized air stimuli are delivered to each end of a linear behavioral arena. Flies walk freely in these arenas, and their position over time, in one odorant or the other, determines their preference score. The arenas are back lit with diffuse IR light, and fly position is tracked automatically from digital video.

B) Schematic of the linear behavioral arenas, into either half of which air odorized with an arbitrary odorant flows. Air is evacuated from the sides of the midpoint of each arena, and the flow is predominantly laminar, resulting in two odor “compartments” with a sharp boundary between them. Flies typically walk back and forth in these arenas, and the fraction of time spent in a reference odor compartment is computed as their preference score.

C) Kymographs showing the position in eight individual flies in eight arenas over time. Color blocks indicate the three minute odor-choice period when the two odors, OCT (magenta) and MCH (green), were delivered. Trajectory reversals at the choice boundary indicate the flies are detecting and responding to the odorants and are largely absent in the pre-odor period (at left). Corresponding preference scores are given at right.

D) Distribution of OCT-MCH preference scores across isogenic wild type animals (iso^{KH11}; see methods). Blue line is the kernel-density estimate of the distribution during the odor-choice period, with shaded area the 95% CI as determined by bootstrapping. Gray line is the corresponding kernel-density estimate during the pre-odor period. Dotted-line distribution indicates the distribution expected under the null hypothesis that all flies exhibit behavior drawn from identical distributions. The null distribution is computed by resampling individual bouts from and back to the choice boundary. The observed distribution is significantly broader than the null distribution ($p < 0.001$; by bootstrap resampling).

E) Scatter plot of individual OCT-MCH odor preferences on day 1 vs individual OCT-MCH odor preferences on day 2. These are significantly correlated ($r = 0.35$; $p < 0.0001$) indicating that individual odor preferences are stable over days. Line is the best linear fit. Shaded region is the 95% CI of the linear fit.

F) Distribution of OCT-, 1-butanol- (BUT), and 2-heptanone- (HEPT) vs-air preference scores. Plot elements as in (D). Bootstrapped *p*-values comparing null and observed distributions were all < 0.001.

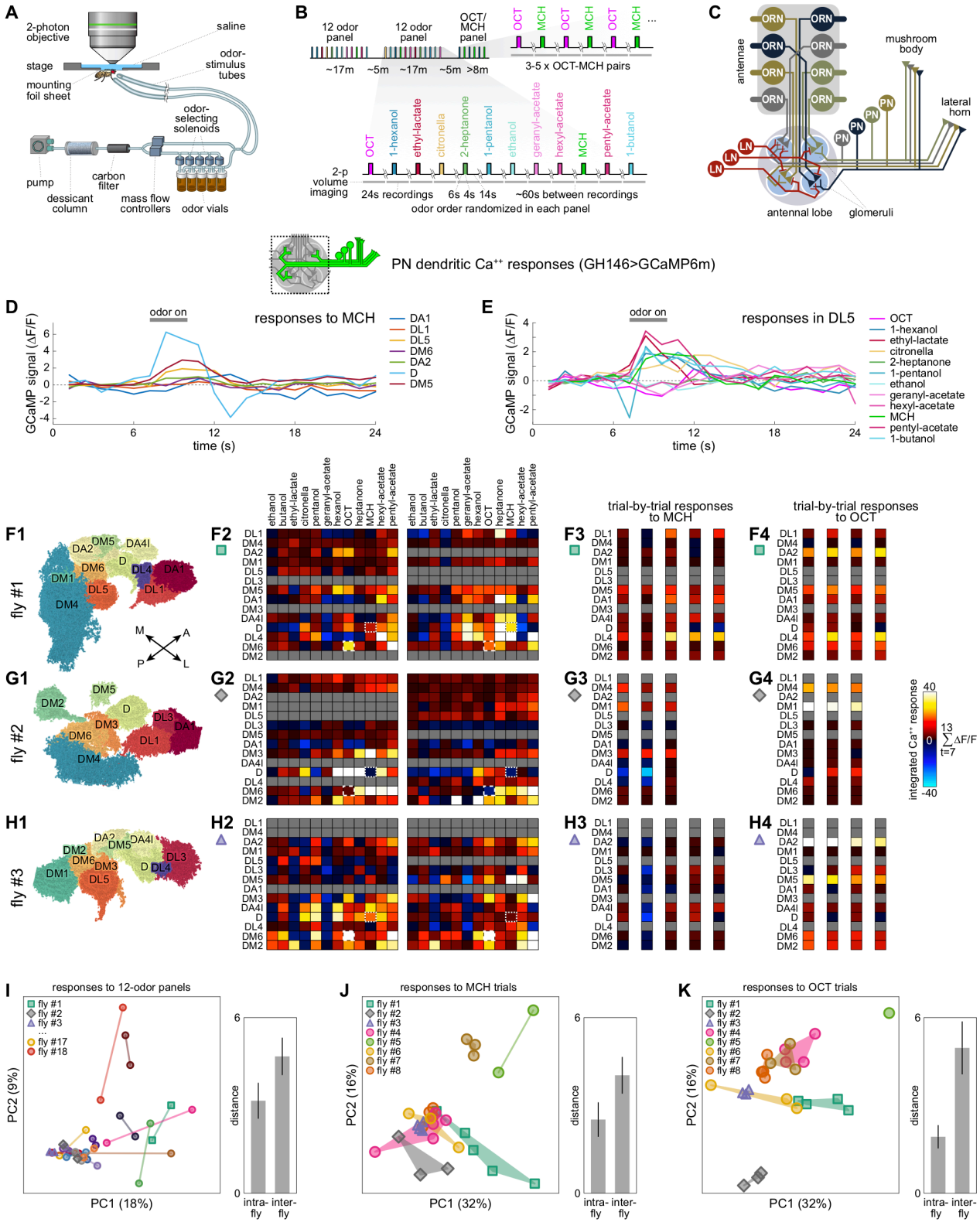
A
2-photon objective
saline
stage
odor-stimulus tubes
mounting foil sheet
odor-selecting solenoids
pump
carbon filter
dessicant column
mass flow controllers
odor vials
B
12 odor panel
12 odor panel
OCT/MCH panel
~17m ~5m ~17m ~5m >8m
3-5 x OCT-MCH pairs
2-p volume imaging
24s recordings 6s 4s 14s ~60s between recordings
odor order randomized in each panel
C
antennae
ORN
PN
LN
mushroom body
lateral horn
antennal lobe
glomeruli
PN dendritic Ca++ responses (GH146>GCaMP6m)
D
responses to MCH
odor on
GCaMP signal (ΔF/F)
time (s)
DA1
DL1
DL5
DM6
DA2
D
DM5
E
responses in DL5
OCT
1-hexanol
ethyl-lactate
citronella
2-heptanone
1-pentanol
ethanol
geranyl-acetate
hexyl-acetate
MCH
pentyl-acetate
1-butanol
F1
fly #1
G1
fly #2
H1
fly #3
F2
G2
H2
F3
trial-by-trial responses to MCH
G3
H3
F4
trial-by-trial responses to OCT
G4
H4
integrated Ca++ response
I
responses to 12-odor panels
PC2 (9%)
PC1 (18%)
distance
intra-fly
inter-fly
J
responses to MCH trials
PC2 (16%)
PC1 (32%)
K
responses to OCT trials

Figure 2 - Individual flies have idiosyncratic odor Ca^{++} responses in the antennal lobe.

A) Schematic of the odor response volumetric imaging set-up. A similar apparatus as used in our behavior assay (Figure 1A) is used to produce an odorized air stimulus under computer control. This is delivered by tubing to a custom stage on which a fly is mounted to a sheet of foil. Its body and head protrude above the foil into a pool of saline under the water-immersion lens of a 2-photon microscope.

B) Schematic of the odor stimuli delivered during an imaging session. First we presented two 12-odor panels, within which the order of odors is randomized in each panel and each odor was presented for 6 seconds. After these panels we stimulated flies with alternating OCT and MCH pulses, starting with OCT or MCH at random. OCT-MCH pairs were repeated up to five times or until the responses ceased.

C) Schematic of the olfactory circuitry from the sensory periphery (olfactory receptor neurons (ORNs) in the antenna) to projection neurons (PNs) bearing odor information into the central brain. LNs are local neurons: predominantly inhibitory interneurons that connect many different sets of glomeruli and inhibit both PNs and LNs, often on the pre-synaptic terminals of ORNs.

D) Ca^{++} responses vs time of seven semiautomatically-segmented glomeruli responding to a pulse of MCH.

E) Ca^{++} responses vs time of the DC3 glomerulus to the 12 odors of the stimulus panel.

F) Ca^{++} from one fly (fly #1). F1) Semiautomatically-segmented glomeruli of the antennal lobe. Voxel clusters (different colors) determined by k-means clustering of odor responses across the stimulus panels (see Methods). Glomerular identity was assigned manually based on the morphology of the glomeruli. F2) Integrated Ca^{++} responses to each odor (columns) of each glomerulus (rows). Two matrices correspond to the two 12-odor panels. Grey cells indicate glomeruli not identified by the semiautomated segmentation pipeline in this fly. Cells with dotted and dashed borders show consistency intra-fly (i.e., between trials) and divergence inter-fly (compare with cells in G and H). F3) Glomerular responses, as in F2, to the MCH trials of the OCT-MCH panel. Colored symbol indicates these data in J) and K). F4) As in F3) but for responses to MCH. Panels F, G and H share the common color axis.

G) As in F), but for fly #2.

H) As in F), but for fly #3.

I) Projection (left) onto principal components 1 and 2 of individual panel responses in the linear space consisting of odor-glomeruli responses (i.e., the 15 glomerulus x 12 odor = 600 dimensional space in which the two matrices of F2 are two data points). Lines connect the two points corresponding to the two 12-odor panels of each fly. n = 18 flies. Right: average distance

among intra-fly trials and inter-fly trials. Bars indicate +/- SEM calculated by 20,000-replicate bootstrap resampling of individuals. p=0.012 by one-tailed resampling of individual flies.

J) As in I), but for responses to MCH (projected from the 15 glomerulus response space in which e.g., F3 and F4 are five and four data points, respectively). Shaded regions are convex hulls containing all the trials from each fly. p=0.002 for intra- vs inter-fly distance comparison.

K) As in J), but for responses to OCT. Shaded regions are convex hulls containing all the trials from each fly. p<0.001 for intra- vs inter-fly distance comparison.

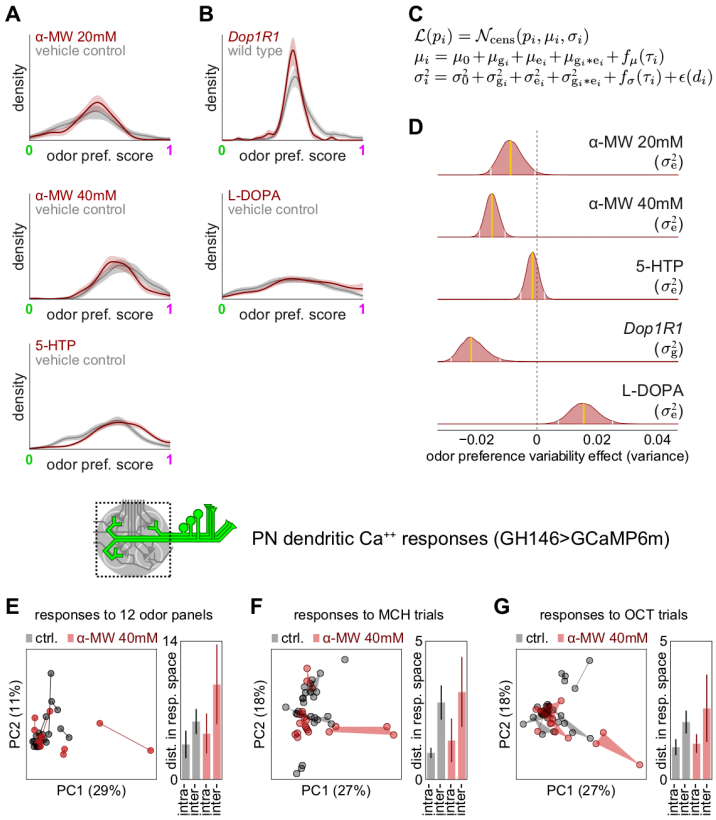

PN dendritic Ca^{++} responses (GH146>GCaMP6m)

Figure 3 - Neuromodulation of behavioral individuality

A) Representative experimental distributions of OCT-MCH preference scores across isogenic wild type animals in control conditions (gray) and fed pharmacological manipulators of serotonin levels (brown). Lines are kernel density estimates of the distributions; shaded areas are the 95% CIs of the density estimates as determined by bootstrapping. Experiments: flies fed 20mM α-MW for three days (top), 40mM α-MW for three days (middle) and 50mM 5-HTP for three days (bottom). Gray lines are matched control conditions. Shaded areas are the 95% CIs of the density estimates as determined by bootstrapping.

B) As in A) for manipulations of dopamine signaling. Top: Kernel-density estimates of the behavioral distribution of *Dop1R1*^{f02676} flies bearing a mutation in the *Dop1R1* dopamine receptor gene and a genetic control. Bottom: observed distributions for flies fed 5mg/mL L-DOPA or vehicle control for three days.

C) Model used to estimate the effects on odor preference variability of neuromodulation manipulations. Briefly, L is the likelihood of observing a particular odor preference p_i, and is distributed as a Normal distribution (modified to account for the data censoring that happens when preference is measured on a 0-1 range) with mean and standard deviation terms that depend on each animal's genotype, environment, the interaction of genotype and environment, and a term to account for seasonal effects of external air temperature. The standard deviation also has a term, ε, that depends on the distance traveled by the fly and accounts for the increased uncertainty in estimating odor preference for inactive flies. See Methods for full explanation.

D) Posterior distributions on the model effects associated with each neuromodulator manipulation. Gold lines indicate the mean of the posterior, and white lines the edges of the 95% credible interval. Posterior distributions heavily overlapping 0 (dotted line) indicate no effect.

E) Left: Projection onto principal components 1 and 2 of individual panel responses in the linear space consisting of odor-glomeruli responses (as in Figure 2I-K). Right: average distance among intra-fly trials and inter-fly trials. Bars indicate +/- SEM calculated by 20,000-replicate bootstrap resampling of individuals. The means within each treatment (intra- vs. inter-) are significantly different ($p=0.011$ and $p=0.024$) by one-tailed resampling. The means between treatments means are not statistically significant ($0.25 < p < 0.35$). Black indicates control flies, brown flies fed 40mM α-MW for three days.

F) As in E) but with points representing responses to MCH in the 15 glomerular space containing MCH and OCT responses (as in Figure 2J and K). As in E), (intra- vs. inter-) means are statistically significant within control treatment ($p = 0.004$) but not statistically significant within

α-MW treatment ($p = 0.093$). The differences in means between treatments means are not statistically significant ($0.34 < p < 0.40$).

G) As in F) but with points representing responses to OCT in the 15 glomerular space containing MCH and OCT responses (as in Figure 2J and K). As in E) and F), means are significantly different within ($p < 0.001$) but not between ($0.34 < p < 0.39$) treatments.

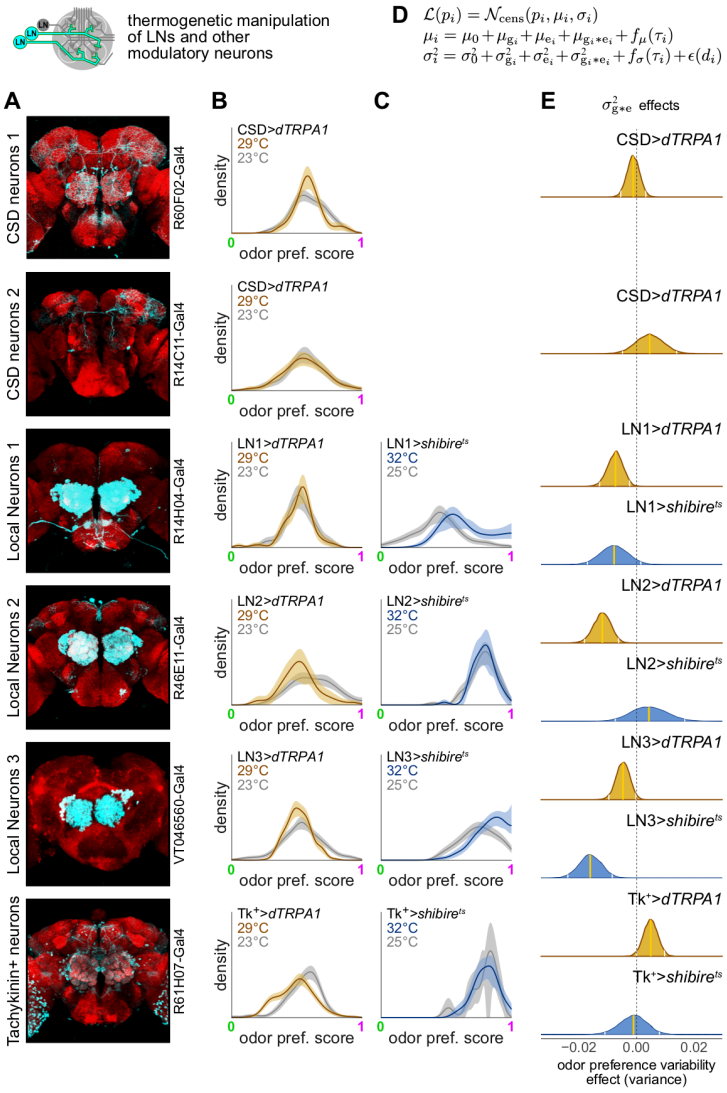
thermogenetic manipulation
of LNs and other
modulatory neurons
D
$\mathcal{L}(p_i) = \mathcal{N}_{\text{cens}}(p_i, \mu_i, \sigma_i)$
$\mu_i = \mu_0 + \mu_{g_i} + \mu_{e_i} + \mu_{g_i * e_i} + f_\mu(\tau_i)$
$\sigma_i^2 = \sigma_0^2 + \sigma_{g_i}^2 + \sigma_{e_i}^2 + \sigma_{g_i * e_i}^2 + f_\sigma(\tau_i) + \epsilon(d_i)$
A
B
C
E
σ^2_{g*e} effects
CSD neurons 1
R60F02-Gal4
CSD neurons 2
R14C11-Gal4
Local Neurons 1
R14H04-Gal4
Local Neurons 2
R46E11-Gal4
Local Neurons 3
VT046560-Gal4
Tachykinin+ neurons
R61H07-Gal4
CSD>dTRPA1
LN1>dTRPA1
LN1>shibire^ts
LN2>dTRPA1
LN2>shibire^ts
LN3>dTRPA1
LN3>shibire^ts
Tk+>dTRPA1
Tk+>shibire^ts
29°C
23°C
32°C
25°C
density
odor pref. score
0
1
−0.02
0.00
0.02
odor preference variability
effect (variance)

Figure 4 - Local neurons in the antennal lobe modulate individuality of odor preference

A) Confocal micrographs of expression patterns targeting the serotonin-immunoreactive CSD neurons, three different populations of local neurons and tachykinin-positive neurons. Red background stain is anti-nc82 staining synaptic active. (The red channel of the VT046560 image is also stained for anti-DLG [56].) Cyan is mCD8-GFP [57] driven by the Gal4 line denoted. Images of all Janelia FlyLight Gal4 lines (all images except that of VT046560) reproduced and modified with permission from the Janelia FlyLight team.

B) Kernel density estimates of the distribution of OCT-MCH preference scores for transgenic animals expressing the thermogenetic activator *dTRPA1*, which depolarizes neurons at 32°C, under the control of each Gal4 driver. Gray distributions are at the permissive temperature (23°C). Gold distributions are at the restrictive temperature (29°C).

C) As in B), but for animals expressing the thermogenetic inhibitor of vesicle release *shibire^{ts}* at permissive (25°C; gray) and restrictive temperatures (32°C; blue).

D) Model used to estimate the effects on odor preference variability of these neural circuit manipulations. The terms of the model are the same as in Figure 3C. Here, the experimental condition terms (*e*) refers to the temperature of the experimental room, and the genotype terms (*g*) account for animals of the background genotype (iso^{KH11}), parental genotype controls (*Gal4*/+, *UAS-shibire^{ts}*/+ and *UAS-dTRPA1*/+), and experimental F_1s (*Gal4*/*UAS-shibire^{ts}* and *Gal4*/*dTRPA1*). The *g*e* term accounts for the thermogenetic interaction of F_1 genotypes and temperature.

E) Posterior distributions of the effect on odor preference variability of silencing (blue) or activating (gold) neurons expressed in each Gal4 line using *shibire^{ts}* or *dTRPA1*, respectively. Gold lines indicate the mean of the posterior, and white lines the edges of the 95% credible interval. Posterior distributions heavily overlapping 0 (dotted line) indicate no effect.

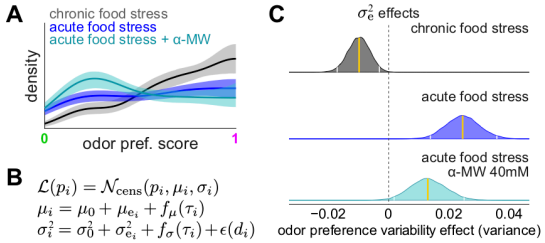
A
chronic food stress
acute food stress
acute food stress + α-MW
density
0
1
odor pref. score
B
$\mathcal{L}(p_i) = \mathcal{N}_{\text{cens}}(p_i, \mu_i, \sigma_i)$
$\mu_i = \mu_0 + \mu_{e_i} + f_\mu(\tau_i)$
$\sigma_i^2 = \sigma_0^2 + \sigma_{e_i}^2 + f_\sigma(\tau_i) + \epsilon(d_i)$
C
σ_e^2 effects
chronic food stress
acute food stress
acute food stress
α-MW 40mM
−0.02
0
0.02
0.04
odor preference variability effect (variance)

Figure 5 - Variability of odor preference is modulated by changes in diet

A) Kernel-density estimates of the behavioral distribution of flies grown chronically on F4-24 flake food (gray), subject to a food stress treatment in which flies were transferred from cornmeal/dextrose food to F4-24 flake food (blue), and flies subject to the same food stress treatment but with 40mM α-MW in both food sources (teal). Shaded areas are 95% CIs.

B) Model used to estimate the effects on odor preference variability of diet manipulations. As these experiments were all conducted with control genotype (iso^{KH11}) animals, there are no *g* terms here compared to the models in Figure 3C and 4D. Otherwise, the terms are comparable.

C) Posterior distributions of the effect of diet manipulations. Gold lines indicate the mean of the posterior, and white lines the edges of the 95% credible interval. Posterior distributions heavily overlapping 0 (dotted line) indicate no effect.

Methods

Data and code repositories

All data needed to reproduce our findings and figures, along with all analysis code is available for download at *http://zenodo.org/REFREF*. These files are also hosted, along with a readme companion page at *http://lab.debivort.org/odor-variability*. Raw imaging files are available on request to the corresponding author.

Fly stocks

The following stocks were obtained from the Bloomington *Drosophila* Stock Center: P{GMR14C11-GAL4}attP2 (BDSC #49256), P{GMR60F02-GAL4}attP2 (#48228), P{GMR61H07-GAL4}attP2 (#39282), P{GMR14H04-GAL4}attP2 (#48665), P{GMR46E11-GAL4}attP2 (#50272), UAS-dTrpA1 (#26263), and P{20XUAS-IVS-GCaMP6m}attP40 (#42748). The VT046650-GAL4 (VDRC ID #204702) driver was obtained from Vienna *Drosophila* Resource Center, and the GH146-GAL4 and *Dop1R1* lines were generously provided by Y. Zhong and J. Dubnau, respectively. The PBac{20XUAS-TTS—shi[ts1]-p10}attP2 line and the split-GAL4 line "MB010B" (13F02-p65ADZp/CyO; 52H09-ZpGdbd) were generously provided by G. Rubin and Y. Aso.

Isogenic line iso^{KH11}

Our main control strain, the isogenic *Drosophila* line iso^{KH11}, was created by inbreeding the balancer-isogenized *w(isoCJ1)* strain of *w^{1118}* ([58]; shared by J. Dubnau) for 10 generations with full-sibling crosses. To equilibrate genetic background, all mutant and transgenic lines listed above were outcrossed to the iso^{KH11} line for at least 10 generations before being used in any imaging or odor preference experiments.

Fly rearing

Unless otherwise indicated, experimental flies were reared in a *Drosophila* incubator (Percival Scientific DR-36VL) under controlled conditions (25°C, 40% RH, 12:12h light:dark cycle) and fed a standardized cornmeal/dextrose medium [59] supplemented with activated yeast. Flies used for behavior were cultured under low-density conditions by allowing ~10 mated females 48-72 hours to lay eggs in a 500ml culture bottle containing folded Kimwipes and ~200ml medium.

Behavioral apparatus

The custom designed behavioral apparatus was constructed of Accura 60 plastic using stereolithography (In'Tech Industries) fabrication. Stainless steel hypo tubing (Small Parts) was used to connect the apparatus with Teflon odor tubes (ID: 0.7mm). The apparatus consisted of 15 parallel tunnels (50mm long, 5mm wide, 1.3mm tall), separated by 5mm spacers. Odorized or clean air was delivered through inlet ports at each end of the tunnel and streams vented to the room through exhaust ports in the center choice zone. Clear acrylic was used as a base and lid for the apparatus. The lid was clamped in place above the apparatus to ensure an air-tight seal during odor presentation. Odors were presented using proportional air blending to control odor concentration. Air dilutions could be made independently for each side of the apparatus. A custom 15-way PEEK manifold was used on each side to split the odorized flow equally between 15 tunnel inlets. A final valve (SH360T041; NResearch) was used immediately upstream of each manifold to quickly switch between pure dehumidified air and the odorized stream. Based on simulation results (details below), airflow through the tunnels is expected to be laminar, and to form a sharp boundary between the two odor compartments at the middle of the corridor.

To maintain a consistent molar flux of odorant at different experimental temperatures, we used digital mass flow controllers to deliver 0.1SLPM air to the end of each tunnel. Because the density of a gas is a function of temperature, the volumetric flow of air increases with temperature to maintain a constant mass flow. Therefore, the velocity of air flowing through the tunnels increases with temperature, but the molar flux of odorant over the fly stays constant (ignoring changes in vapor pressure). The laminar air velocity in the direction of the center port was approximately 2.6cm/sec at 25°C, well within the range of wind speeds experienced by insects in a natural environment [60].

A three-dimensional Computational Fluid Dynamics (CFD) analysis was performed using Autodesk CFD (Autodesk, Inc., San Rafael, CA) software to model the flow of gas through the tunnels. CFD analysis revealed that flow through most of the length of each tunnel is laminar, with some turbulent flow in the center and near the inlet ports on each end (Figure S1A). A scalar mixing simulation, using a simulated tracer gas, revealed a steep mixing gradient for odor concentration, limited almost entirely to the center choice zone where the opposing odor streams meet (Figure S1B). These results are in general agreement with the behavior we observe.

Odor delivery

For imaging experiments, odors were delivered using a 12-channel serial-air-dilution olfactometer described in [61]. For behavioral experiments, odors were presented using a dual-path odor delivery system integrated into the behavioral apparatus. In both devices, desiccated air was filtered through an

activated carbon trap (Agilent HT-200) before passing through digital mass flow controllers (MFCs; Alicat Scientific). For each odorant, 5ml of pure odorant was placed with a folded strip of filter paper in a 40ml glass vial fitted with a custom PTFE cap with inert fittings. The saturated headspace from these vials was combined with a variable carrier stream to produce between 10% and 20% saturated vapor, the range in which we observe a linear input-output relationship. All tubing was pure PTFE or PTFE coated for inertness. A photoionization detector (200B miniPID, Aurora Scientific) was used to periodically monitor the concentrations of test odors being delivered. The following odorants were obtained from Sigma-Aldrich: 2-heptanone (CAS#: 110-43-0), 1-pentanol (71-41-0), 3-octanol (589-98-0), hexyl-acetate (142-92-7), 4-methylcyclohexanol (589-91-3), pentyl-acetate (628-63-7), 1-butanol (71-36-3), ethyl-lactate (97-64-3), geranyl acetate (105-87-3), and 1-hexanol (111-27-34). Citronella and peppermint essential oils were purchased from Aura Cacia (items #191112 and #188840), and 200 proof ethanol from Decon Labs (V1001).

Behavior imaging

Flies were illuminated from beneath using a modified 15-inch laptop display panel (LP150X2; LG Philips) equipped with a high-density infrared LED array (peak emission 880nm). This approach produces homogeneous backlighting for high-contrast silhouette detection at a wavelength not visible to the fly. The screen was placed approximately 4cm below the behavioral apparatus to avoid heating the flies. We used a high-resolution CMOS camera (Point Grey Firefly MV USB) equipped with a zoom lens and longpass filter (Kodak Wratten Filter #87C) to collect images at 60Hz.

Behavior-tracking software

Custom MATLAB (The MathWorks, Inc.) routines were used to record and analyze the behavior of flies and control odor delivery. Tunnels and flies were automatically detected using 2D cross-correlation to align tunnel and fly outlines to template images. During an odor experiment, each frame was background subtracted to yield the silhouettes of the flies being assayed. For each time point, the centroid position, orientation, and major axis length of each silhouette were calculated and stored for offline analysis.

Behavioral experiments

Flies to be assayed for behavior were collected within 24 hours of eclosing and placed into a fresh vial containing fresh cornmeal/dextrose medium. Strictly, only females were used for behavior and imaging experiments. Vials each contained approximately 30 female flies, and were kept in the temperature and humidity-controlled incubator for 3 days, so that all flies were 3-4 days post-exclusion when tested. Flies were individually aspirated into the behavioral apparatus through a small hole in the lid. No

anesthesia was used at any point on flies used in behavioral experiments. To minimize external causes of behavioral variability, odor preference assays were performed in an isolated temperature-controlled environmental chamber in total darkness. Behavioral assays began immediately after all flies were loaded and the lights were turned off. Each odor preference experiment ran for a total of 6 minutes and 30 seconds: 3 minutes of clean air, 3 minutes of air mixed with odorant, and 30 seconds of clean air post-odorant. The apparatus was partially disassembled and wiped down with absolute ethanol between experiments to remove any fly-deposited contamination. Prior to running behavioral experiments we adjusted odor concentrations so that the mean odor preference for OCT would be near 0.4. This was done by measuring the mean odor preference of a small number of iso^{KH11} flies prior to the behavior experiment, then adjusting concentrations via flow controllers and remeasuring mean preference.

Preference persistence experiments

Several experiments required storing and maintaining identities of individual flies across multiple days. For this we used FlyPlates (FlySorter LLC, Seattle, WA), which are modified 96-well plates with a mesh top and bottom. The plates were placed on a bed of cornmeal/dextrose fly medium and individual flies were aspirated into and out of each well, allowing identities to be maintained across multiple days. The food was replaced daily. To remove any potential contribution of between-tunnel differences in stimulus delivery to the across-day correlation, the tunnel assignment for each fly was randomly chosen each day.

Gal4 expression pattern images

Panels modified with permission from FlyLight images (Figure 4A) were downloaded from http://flweb.janelia.org/cgi-bin/flew.cgi. Confocal micrographs of expression patterns targeting, the red is the background stain for anti-nc82, and cyan is mCD8-GFP.

Calcium Imaging fly prep

Flies were collected from population bottles within 24 hours of eclosion. Those flies were put into vials with standard cornmeal/dextrose fly food for approximately 72 hours. Prior to mounting, single flies were cold anesthetized by being sealed in a plastic tube and submerged in ice. The anesthetized fly was then placed into a custom platform that exposed the fly head for removal of the cuticle and calcium imaging of the antennal lobe while keeping the antennae dry and exposed beneath the platform. The platform was a 3D printed 80mm diameter circle with a 5mm by 5mm square recessed into the center. At the bottom of the recess was a thin aluminum sheet (0.5mm) with a laser cut hole which allowed for the fly's head and thorax to be wedged between to stabilize the fly without damage. The fly's head was

fixed to the stage by applying a small amount of UV (Loctite AA 3972) curing glue around the edge of both eyes to secure it the stage. The proboscis was then carefully extended and waxed to the bottom of the stage to further prevent movement of the head. We used a saline solution, as described in the methods of [62], to cover the exposed fly head and thorax and filling the small recessed section of the mounting stage. We used a sharpened 32-gauge needle to cut the cuticle of the fly and expose the antennal lobe.

Calcium imaging

GCaMP6m-expressing flies were imaged using a custom-built galvanometer-scanning two-photon microscope and ultrafast Ti:sapphire laser (Spectra-Physics Mai Tai) tuned to 930 nm. The microscope was controlled with a customized build of ScanImage 3.8 software (Vidrio Technologies, [63]). Custom MATLAB scripts were used to control stimulus delivery during imaging. Fast volume-scanning was performed using a piezoelectric objective scanner (Physik Instrumente PIFOC PD72Z4), capable of continuous sawtooth movement in the Z dimension. Each volume was imported as a tiff stack and smoothed with a 3-dimensional gaussian kernel with standard deviation of 3 in all dimensions. A background was selected for every odor presentation by pooling all volumes and taking pixels with intensity below the 25th percentile. This background mask was applied to the volumes to get a mean value across time for background subtraction. The volumes represented by a 3-dimensional matrix of voxel values were converted to a one-dimensional vector and stacked together across time to create the matrix for *k*-means clustering (n-voxels by *k*-time points). Each voxel was *z*-scored across time and *k*-means clustering was run using MATLAB R2018a's default KMEANS function with k = 36 and replicates = 15. For each cluster output by *k*-means, we applied a lenient size criterion that included only clusters composed of between 300 and 30,000 voxels. We then manually sorted through the remaining clusters to pick those that look reasonable in terms of geometry, size, and location, using a 3-dimensional *in-vivo Drosophila* antennal lobe atlas as a guide [64]. The selected clusters represented the glomeruli for each fly. This glomerulus mask was applied to the fly's odor block to yield $\Delta F/F$ traces for each glomerulus-odor pair within the fly. Within a single fly, separate *k*-means glomeruli masks were generated and applied for each odor presentation block (12-odor block-1, 12-odor block-2, and the block of OCT/MCH presentations). The matrix for principal component analysis was created by taking the integrated sum of $\Delta F/F$ for seconds 7-13 for each glomerulus-odor pair in an odor block, and z-scoring across flies. Whenever a glomerulus cannot be identified within a fly, the associated glomerulus-odor values for that fly are considered missing data. For our PCA matrix, we replaced any missing data within a fly with the mean across all flies of that specific odor-glomerulus value.

Thermogenetics

The thermogenetic effectors, UAS-shibire^{ts} and UAS-dTrpA1, were obtained from Bloomington Stock Center and backcrossed for at least ten generations into our isogenic line *iso^{KH11}*. For behavioral experiments, each effector was crossed to a GAL4 driver line and F_1s were used for the experiment. TrpA1 F_1s were tested at 23°C (permissive temperature control condition) or 29°C (restrictive; TRPA1 active). Shibire^{ts} F_1s were tested at 25°C (permissive temperature control condition) or at 32°C (restrictive; Shibire^{ts} blocking vesicle release). Animals in the restrictive condition were incubated for 30 minutes at 32°C prior to testing.

Pharmacology

Flies used for drug treatment experiments were placed on food that was supplemented with either α-MW, 5-htp, or L-DOPA. To create the drug food mixture, the drug was mixed into water solution and diluted to the appropriate concentration with melted cornmeal/dextrose standard medium or F4-24 flake food, then placed into an empty plastic vial (Genesee scientific 32-116). The flies were flipped onto freshly made drug-supplemented food daily for the 72 hours post eclosion.

Food-induced environmental stress

Formula 4-24 (F4-24) prepared food mix was purchased from Carolina Biological Supply Company (item #173120). Portions of this dry media mix were processed in a coffee grinder to achieve a uniform density and mixed with tap water with a ratio of 1:1. For the food shock experiments we placed newly eclosed flies onto cornmeal/dextrose medium for 48 hours, then switched to F4-24 food for the remaining 24 hours prior to evaluating behavior.

Behavioral analysis

All behavioral analyses were performed using R-3.5.1 [65] or MATLAB R2018b. Behavioral analyses consisted of both model-based (estimating effects of experimental manipulations) and non model-based (individuality scores and distribution visualizations) inference. For non model-based analyses we included only flies that met a minimum activity threshold of 25 cm of distance traveled during the odor period, since highly inactive flies can substantially skew the analysis. For model-based analyses we adjust for group differences in activity level, so we included all flies that entered the choice zone of the tunnel at least once during the experiment.

Individuality scores were calculated as Var_{obs} - Var_{null}. Though MAD as a measure of dispersion is preferable to variance, as discussed below, we used variance to estimate individuality because its additive property makes the numerical difference between observed and null a meaningful quantity. The

individuality score is interpretable as the amount of additional variance, supplied by stable inter-fly preference differences, beyond that expected from sampling error alone.

The expected “null model” variance was estimated from a distribution derived by Monte Carlo simulation. Briefly, we calculated a transition matrix representing the proportion of times flies crossed from one odor into the other, or entered the choice zone and then returned to the side they came from. Then we segmented tunnel position traces into a series of bout times - the time between entering an odorized portion of the tunnel and leaving it, and pooled them together according to odor. For a given group of flies, the collection of odor bouts preserves the overall mean preference, but discards the correlation of bouts observed within a fly. A population of virtual “Markov flies” equal to the number of observed flies was generated and each virtual fly was assigned an initial “odor choice.” For each virtual fly, a Markov chain of choices was generated from the empirical transition matrix, and each virtual choice was paired with an occupancy time sampled from the pool of bout times for its respective odor. Samples were repeatedly taken from the chain until 3 minutes of simulated behavior was collected for each fly. From each Markov fly’s simulated time series, we calculated the proportion of time spent in the reference odor and collected these preference scores across the virtual population. This procedure was repeated 1,000 times and the variance of simulated scores across each virtual population was calculated. From this distribution of simulated variances, 10,000 bootstrap replicates were taken and used to estimate confidence intervals and p-values of the null hypothesis test of no difference between the variance of the observed and the simulated preference scores.

Modeling of behavioral effects

Our goal was to measure the effect size of specific experimental manipulations on inter-fly odor preference variability. Isolating these effects is difficult for several reasons. First, observed behavioral variance is confounded by sampling error. To minimize the impact of sampling error, we could simply sample odor responses for a longer period of time; however, after several minutes, most flies adapt to the stimuli and behaviorally habituate. Second, manipulating environmental temperature and neural activity may produce changes in overall locomotor activity. This issue directly impacts the sampling error issue, since less active animals will have fewer chances to cross the center and sample both odors, thus biasing preference scores toward extreme values. Third, our measure of preference, a proportion, is bounded on [0,1], which tends to artificially deflate estimates of dispersion. Indeed, variance is a poor measure of dispersion on bounded distributions because it is not robust to accumulated observations at the extrema. Furthermore, we believe that it is unlikely that two flies with a measured odor preference of e.g., 1, truly have the exact same magnitude of preference. Rather, our assay is incapable of resolving these differences because of sampling limitations, a phenomenon

generally known as data censoring. These issues are further exacerbated when the mean is far from 0.5, causing more flies to accumulate at values of 0 or 1, thereby producing an artificial dependence of dispersion on the central tendency. Thus, we must be concerned that experimental manipulations which affect the mean can amplify the censoring effect and produce spurious apparent effects on variance. One possible way to address these concerns is to use non-parametric measure of dispersion, e.g., MAD or IQR, as done previously [20]. However, that only addresses the issue of measuring dispersion in a robust way. To address the other issues we must control for the confounding effects of overall locomotor activity on measured preference.

We used a linear modeling approach to address these challenges by jointly modeling the main effects of experimental manipulations, their interactions, and confounding "nuisance" parameters on both the mean and variance of odor preference scores. We developed a novel censored heteroscedastic regression model, where experimental and environmental factors exert their effects on odor preference distribution independently and in combination. For example, preference variability in experiments utilizing thermogenetic reagents was potentially affected by two factors we would like to control for (genotype and experimental temperature) and by their interaction, which is the effect size we are actually interested in estimating [66]. The likelihood, *L,* of observing a particular odor preference, p_i, is calculated from a censored Normal distribution:

$$\mathcal{L}(p_i) = \mathcal{N}_{cens}(p_i, \mu_i, \sigma_i)$$

which assumes that the odor preference is a latent continuous variable and that observed values of 0 and 1 are really censored observations of preference values that extend beyond the observable range [0,1]. The formulation of odor preference as a censored latent variable makes the estimation of variance in the model insensitive to changes in the mean. The expected mean, μ, and standard deviation, σ, of odor preference for fly *i*:

$$\mu_i = \mu_0 + \mu_{g_i} + \mu_{e_i} + \mu_{g_i * e_i} + f_\mu(\tau_i)$$

$$\sigma_i^2 = \sigma_0^2 + \sigma_{g_i}^2 + \sigma_{e_i}^2 + \sigma_{g_i * e_i}^2 + f_\sigma(\tau_i) + \epsilon(d_i)$$

depend on animal *i*'s genotype, environment, the interaction of genotype and environment (coded as binary indicator variables), and a term to account for seasonal effects of external air temperature (a scaled continuous variable). The standard deviation has an offset term, ε, defined for a given fly as:

$$\epsilon_i = a * dist_i^b + c$$

that depends on the distance, *dist*, traveled by fly *i* during the odor period and accounts for the increased uncertainty in estimating odor preference for inactive flies. The relationship between ε and *dist* was determined empirically by fitting a function, of the form shown in Eq. 3, to the pre-odor

variance-by-distance plot of a pilot dataset (Figure S1D). The coefficient values used in all three models were a = 2.365, b = -0.651, c = -0.0077.

As shown above, we included two nuisance terms in the model to adjust for uncontrolled sources of variability: an offset to the variance based on the distance traveled during the odor period, and an additional uncontrolled environmental variable (the average air temperature in Boston) that was observed to have a significant association with preference variability (Figure S6B,D). Air temperature data recorded at the Boston Logan International Airport weather station (WBAN:14739) were downloaded from the NOAA Climate Data Online website [66] for the time period encompassing our behavior experiments. Temperature values were scaled to have a mean of 0 and a standard deviation of 1.

Bayesian model fitting

The model described above may be fit using maximum likelihood estimation or by using Markov Chain Monte Carlo (MCMC) simulation within a Bayesian framework. We chose to use the Bayesian approach, since the inclusion of reasonable prior expectations can provide parameter regularization and aid in model identifiability. Models were programmed in the Stan modeling language [67,68] and implemented using the RStan library for R [69]. Model fitting was performed on the Odyssey cluster supported by the FAS Division of Science, Research Computing Group at Harvard University.

For each model, 32 MCMC chains were run in parallel using the No-U-Turn-Sampler implementation of the Hamiltonian Monte Carlo algorithm [70]. Briefly, 1,500 samples were drawn from each chain, and the first 1,000 warm-up samples were discarded. The remaining 500 samples from each chain were aggregated, for a total of 16,000 samples taken from the joint posterior. Several within-chain and between-chain diagnostic criteria were monitored for each model, in accordance with current best practices [71]. These diagnostics did not indicate any pathological MCMC behaviors for any of the models reported.

A series of pilot experiments using the control genotype (iso^{KH11}) under baseline conditions was used to update an initial set of vague priors on the mean intercept, variance intercept, and environmental air temperature coefficient terms in the model (n = 3,722 flies total). The posterior standard deviations (multiplied by a factor of ten to reflect more uncertainty) and means from this model were used as prior parameter values for their corresponding terms in subsequent models:

$$\mu_0 \sim \mathcal{N}(0.5, 0.25)$$
$$\sigma_0^2 \sim \mathcal{N}(0.012, 0.01)$$
$$f_\mu \sim \mathcal{N}(-0.034, 0.03)$$
$$f_\sigma \sim \mathcal{N}(-0.008, 0.01)$$

For all regression coefficient priors, we used a Normal distribution, centered at 0, and selected weakly-informative, but reasonable, values for the scale:

$$\mu_g \sim \mathcal{N}(0, 0.2)$$
$$\mu_e \sim \mathcal{N}(0, 0.2)$$
$$\mu_{g*e} \sim \mathcal{N}(0, 0.2)$$
$$\sigma_g^2 \sim \mathcal{N}(0, 0.01)$$
$$\sigma_e^2 \sim \mathcal{N}(0, 0.01)$$
$$\sigma_{g*e}^2 \sim \mathcal{N}(0, 0.01)$$

The overall goal for selecting priors was simply to provide some degree of regularization for parameter estimates and to aid in model identifiability, rather than to influence posterior estimates based on any prior expectations about specific effects. We fit a total of three separate regression models for: 1) neuromodulation experiments shown in Figures 3 and 5 (n = 5,327 flies total); 2) thermogenetic experiments using the *dTrpA1* effector in Figure 4 (n = 5,285); and 3) thermogenetic experiments using the *shi^{ts1}* effector in Figure 4 (n = 2,027).

Kernel Density Estimates (KDE) of odor preference distributions

The KDEs of odor preference were estimated in MATLAB using the KSDENSITY function with a Gaussian kernel. Kernel bandwidth was automatically chosen using the default optimal method for normal densities, and censoring was applied at values of 0 and 1, the upper and lower bounds of observable odor preference scores.

Acknowledgements

We are thankful to Katrin Vogt and Carolyn Elya for helpful comments on the manuscript. We also thank Ed Soucy and Joel Greenwood of Harvard's CBS Neuroengineering core for their assistance with construction of the two-photon microscope, along with Jess Kanwal and Kyobi Skutt-Kakaria for insightful discussions. BdB was supported by a Sloan Research Fellowship, a Klingenstein-Simons

Fellowship Award, a Smith Family Odyssey Award, and the National Science Foundation under grant no. IOS-1557913. GT was supported by the Howard Hughes Medical Institute.

Conflicts

BdB is a scientific advisor for FlySorter, LLC. The authors have no additional conflicts.

References

1. Keller, Andreas, Richard C. Gerkin, Yuanfang Guan, Amit Dhurandhar, Gabor Turu, Bence Szalai, Joel D. Mainland, et al. 2017. “Predicting Human Olfactory Perception from Chemical Features of Odor Molecules.” *Science* 355 (6327): 820–26.
2. Koulakov, Alexei A., Brian E. Kolterman, Armen G. Enikolopov, and Dmitry Rinberg. 2011. “In Search of the Structure of Human Olfactory Space.” *Frontiers in Systems Neuroscience* 5 (September): 65.
3. Secundo, Lavi, Kobi Snitz, and Noam Sobel. 2014. “The Perceptual Logic of Smell.” *Current Opinion in Neurobiology* 25 (April): 107–15.
4. Distel, H., S. Ayabe-Kanamura, M. Martínez-Gómez, I. Schicker, T. Kobayakawa, S. Saito, and R. Hudson. 1999. “Perception of Everyday Odors--Correlation between Intensity, Familiarity and Strength of Hedonic Judgement.” *Chemical Senses* 24 (2): 191–99.
5. Keller, Andreas, Margaret Hempstead, Iran A. Gomez, Avery N. Gilbert, and Leslie B. Vosshall. 2012. “An Olfactory Demography of a Diverse Metropolitan Population.” *BMC Neuroscience* 13 (October): 122.
6. Keller, Andreas, and Leslie B. Vosshall. 2016. “Olfactory Perception of Chemically Diverse Molecules.” *BMC Neuroscience* 17 (1): 55.
7. Keller, Andreas, Hanyi Zhuang, Qiuyi Chi, Leslie B. Vosshall, and Hiroaki Matsunami. 2007. “Genetic Variation in a Human Odorant Receptor Alters Odour Perception.” *Nature* 449 (7161): 468–72.
8. Mainland, Joel D., Andreas Keller, Yun R. Li, Ting Zhou, Casey Trimmer, Lindsey L. Snyder, Andrew H. Moberly, et al. 2014. “The Missense of Smell: Functional Variability in the Human Odorant Receptor Repertoire.” *Nature Neuroscience* 17 (1): 114–20.
9. Menashe, Idan, Tatjana Abaffy, Yehudit Hasin, Sivan Goshen, Vered Yahalom, Charles W. Luetje, and Doron Lancet. 2007. “Genetic Elucidation of Human Hyperosmia to Isovaleric Acid.” *PLoS Biology* 5 (11): e284.
10. Couto, Africa, Mattias Alenius, and Barry J. Dickson. 2005. “Molecular, Anatomical, and Functional Organization of the Drosophila Olfactory System.” *Current Biology: CB* 15 (17): 1535–47.
11. Fishilevich, Elane, and Leslie B. Vosshall. 2005. “Genetic and Functional Subdivision of the Drosophila Antennal Lobe.” *Current Biology: CB* 15 (17): 1548–53.
12. Laissue, Philippe P., and Leslie B. Vosshall. 2008. “The Olfactory Sensory Map in Drosophila.” *Advances in Experimental Medicine and Biology* 628: 102–14.
13. Lin, Hui-Hao, Jason Sih-Yu Lai, An-Lun Chin, Yung-Chang Chen, and Ann-Shyn Chiang. 2007. “A Map of Olfactory Representation in the Drosophila Mushroom Body.” *Cell* 128 (6): 1205–17.
14. Jefferis, Gregory S. X. E., Christopher J. Potter, Alexander M. Chan, Elizabeth C. Marin, Torsten Rohlfing, Calvin R. Maurer Jr, and Liqun Luo. 2007. “Comprehensive Maps of Drosophila Higher

Olfactory Centers: Spatially Segregated Fruit and Pheromone Representation." *Cell* 128 (6): 1187–1203.

15. Fişek, Mehmet, and Rachel I. Wilson. 2014. "Stereotyped Connectivity and Computations in Higher-Order Olfactory Neurons." *Nature Neuroscience* 17 (2): 280–88.
16. Chou, Ya-Hui, Maria L. Spletter, Emre Yaksi, Jonathan C. S. Leong, Rachel I. Wilson, and Liqun Luo. 2010. "Diversity and Wiring Variability of Olfactory Local Interneurons in the Drosophila Antennal Lobe." *Nature Neuroscience* 13 (4): 439–49.
17. Seki, Yoichi, Jürgen Rybak, Dieter Wicher, Silke Sachse, and Bill S. Hansson. 2010. "Physiological and Morphological Characterization of Local Interneurons in the Drosophila Antennal Lobe." *Journal of Neurophysiology* 104 (2): 1007–19.
18. Tanaka, Nobuaki K., Keita Endo, and Kei Ito. 2012. "Organization of Antennal Lobe-Associated Neurons in Adult Drosophila Melanogaster Brain." *The Journal of Comparative Neurology* 520 (18): 4067–4130.
19. Kim, Susy M., Chih-Ying Su, and Jing W. Wang. 2017. "Neuromodulation of Innate Behaviors in Drosophila." *Annual Review of Neuroscience* 40 (July): 327–48.
20. Kain, Jamey S., Chris Stokes, and Benjamin L. de Bivort. 2012. "Phototactic Personality in Fruit Flies and Its Suppression by Serotonin and White." *Proceedings of the National Academy of Sciences of the United States of America* 109 (48): 19834–39.
21. Buchanan, Sean M., Jamey S. Kain, and Benjamin L. de Bivort. 2015. "Neuronal Control of Locomotor Handedness in Drosophila." *Proceedings of the National Academy of Sciences of the United States of America* 112 (21): 6700–6705.
22. Kain, Jamey S., Sarah Zhang, Jamilla Akhund-Zade, Aravinthan D. T. Samuel, Mason Klein, and Benjamin L. de Bivort. 2015. "Variability in Thermal and Phototactic Preferences in Drosophila May Reflect an Adaptive Bet-Hedging Strategy : BET-HEDGING EXPLAINS THERMOTACTIC VARIABILITY." *Evolution; International Journal of Organic Evolution* 69 (12): 3171–85.
23. Todd, Jeremy G., Jamey S. Kain, and Benjamin L. de Bivort. 2017. "Systematic Exploration of Unsupervised Methods for Mapping Behavior." *Physical Biology* 14 (1): 015002.
24. Honegger, Kyle, and Benjamin de Bivort. 2018. "Stochasticity, Individuality and Behavior." *Current Biology: CB* 28 (1): R8–12.
25. Linneweber, G., M. Andriatsilavo, S. Dutta, and L. Hellbruegge. 2019. "A Neurodevelopmental Origin of Behavioral Individuality." *bioRxiv*. https://www.biorxiv.org/content/10.1101/540880v1.abstract.
26. Sizemore, Tyler R., and Andrew M. Dacks. 2016. "Serotonergic Modulation Differentially Targets Distinct Network Elements within the Antennal Lobe of Drosophila Melanogaster." *Scientific Reports* 6 (November): 37119.

27. Ayroles, Julien F., Sean M. Buchanan, Chelsea O'Leary, Kyobi Skutt-Kakaria, Jennifer K. Grenier, Andrew G. Clark, Daniel L. Hartl, and Benjamin L. de Bivort. 2015. "Behavioral Idiosyncrasy Reveals Genetic Control of Phenotypic Variability." *Proceedings of the National Academy of Sciences of the United States of America* 112 (21): 6706–11.

28. Claridge-Chang, Adam, Robert D. Roorda, Eleftheria Vrontou, Lucas Sjulson, Haiyan Li, Jay Hirsh, and Gero Miesenböck. 2009. "Writing Memories with Light-Addressable Reinforcement Circuitry." *Cell* 139 (2): 405–15.

29. Dierick, Herman A., and Ralph J. Greenspan. 2007. "Serotonin and Neuropeptide F Have Opposite Modulatory Effects on Fly Aggression." *Nature Genetics* 39 (5): 678–82.

30. Riemensperger, Thomas, Guillaume Isabel, Hélène Coulom, Kirsa Neuser, Laurent Seugnet, Kazuhiko Kume, Magali Iché-Torres, et al. 2011. "Behavioral Consequences of Dopamine Deficiency in the Drosophila Central Nervous System." *Proceedings of the National Academy of Sciences of the United States of America* 108 (2): 834–39.

31. Kim, Young-Cho, Hyun-Gwan Lee, and Kyung-An Han. 2007. "D1 Dopamine Receptor dDA1 Is Required in the Mushroom Body Neurons for Aversive and Appetitive Learning in Drosophila." *The Journal of Neuroscience: The Official Journal of the Society for Neuroscience* 27 (29): 7640–47.

32. Lebestky, Tim, Jung-Sook C. Chang, Heiko Dankert, Lihi Zelnik, Young-Cho Kim, Kyung-An Han, Fred W. Wolf, Pietro Perona, and David J. Anderson. 2009. "Two Different Forms of Arousal in Drosophila Are Oppositely Regulated by the Dopamine D1 Receptor Ortholog DopR via Distinct Neural Circuits." *Neuron* 64 (4): 522–36.

33. Szyszka, Paul, Christiane Demmler, Mariann Oemisch, Ludwig Sommer, Stephanie Biergans, Benjamin Birnbach, Ana F. Silbering, and C. Giovanni Galizia. 2011. "Mind the Gap: Olfactory Trace Conditioning in Honeybees." *The Journal of Neuroscience: The Official Journal of the Society for Neuroscience* 31 (20): 7229–39.

34. Ko, Kang I., Cory M. Root, Scott A. Lindsay, Orel A. Zaninovich, Andrew K. Shepherd, Steven A. Wasserman, Susy M. Kim, and Jing W. Wang. 2015. "Starvation Promotes Concerted Modulation of Appetitive Olfactory Behavior via Parallel Neuromodulatory Circuits." *eLife* 4 (July). https://doi.org/10.7554/eLife.08298.

35. Hamada, Fumika N., Mark Rosenzweig, Kyeongjin Kang, Stefan R. Pulver, Alfredo Ghezzi, Timothy J. Jegla, and Paul A. Garrity. 2008. "An Internal Thermal Sensor Controlling Temperature Preference in Drosophila." *Nature* 454 (7201): 217–20.

36. Sykes, Paul A., and Barry G. Condron. 2005. "Development and Sensitivity to Serotonin of Drosophila Serotonergic Varicosities in the Central Nervous System." *Developmental Biology* 286 (1): 207–16.

37. Kitamoto, T. 2001. “Conditional Modification of Behavior in Drosophila by Targeted Expression of a Temperature-sensitive Shibire Allele in Defined Neurons.” *Journal of Neurobiology*. https://onlinelibrary.wiley.com/doi/abs/10.1002/neu.1018.
38. Asahina, Kenta, Kiichi Watanabe, Brian J. Duistermars, Eric Hoopfer, Carlos Roberto González, Eyrún Arna Eyjólfsdóttir, Pietro Perona, and David J. Anderson. 2014. “Tachykinin-Expressing Neurons Control Male-Specific Aggressive Arousal in Drosophila.” *Cell* 156 (1-2): 221–35.
39. Parnas, Moshe, Andrew C. Lin, Wolf Huetteroth, and Gero Miesenböck. 2013. “Odor Discrimination in Drosophila: From Neural Population Codes to Behavior.” *Neuron* 79 (5): 932–44.
40. Das, Sudeshna, Madhumala K. Sadanandappa, Adrian Dervan, Aoife Larkin, John Anthony Lee, Indulekha P. Sudhakaran, Rashi Priya, et al. 2011. “Plasticity of Local GABAergic Interneurons Drives Olfactory Habituation.” *Proceedings of the National Academy of Sciences of the United States of America* 108 (36): E646–54.
41. Bhandawat, Vikas, Shawn R. Olsen, Nathan W. Gouwens, Michelle L. Schlief, and Rachel I. Wilson. 2007. “Sensory Processing in the Drosophila Antennal Lobe Increases Reliability and Separability of Ensemble Odor Representations.” *Nature Neuroscience* 10 (11): 1474–82.
42. Schulz, David J., Jean-Marc Goaillard, and Eve Marder. 2006. “Variable Channel Expression in Identified Single and Electrically Coupled Neurons in Different Animals.” *Nature Neuroscience* 9 (3): 356–62.
43. Stern, Shay, Christoph Kirst, and Cornelia I. Bargmann. 2017. “Neuromodulatory Control of Long-Term Behavioral Patterns and Individuality across Development.” *Cell* 171 (7): 1649–62.e10.
44. Mansourian, Suzan, Anders Enjin, Erling V. Jirle, Vedika Ramesh, Guillermo Rehermann, Paul G. Becher, John E. Pool, and Marcus C. Stensmyr. 2018. “Wild African Drosophila Melanogaster Are Seasonal Specialists on Marula Fruit.” *Current Biology: CB* 28 (24): 3960–68.e3.
45. Becher, Paul G., Gerhard Flick, Elżbieta Rozpędowska, Alexandra Schmidt, Arne Hagman, Sébastien Lebreton, Mattias C. Larsson, et al. 2012. “Yeast, Not Fruit Volatiles Mediate Drosophila Melanogaster Attraction, Oviposition and Development.” Edited by Ken Thompson. *Functional Ecology* 26 (4): 822–28.
46. Austin, Christopher J., Christopher G. Guglielmo, and Amanda J. Moehring. 2014. “A Direct Test of the Effects of Changing Atmospheric Pressure on the Mating Behavior of Drosophila Melanogaster.” *Evolutionary Ecology* 28 (3): 535–44.
47. Zhang, Xiaonan, and Quentin Gaudry. 2016. “Functional Integration of a Serotonergic Neuron in the Drosophila Antennal Lobe.” *eLife* 5 (August). https://doi.org/10.7554/eLife.16836
48. Olsen, Shawn R., Vikas Bhandawat, and Rachel I. Wilson. 2010. “Divisive Normalization in Olfactory Population Codes.” Neuron 66 (2): 287–99.

49. Qin, Hongtao, Michael Cressy, Wanhe Li, Jonathan S. Coravos, Stephanie A. Izzi, and Joshua Dubnau. 2012. “Gamma Neurons Mediate Dopaminergic Input during Aversive Olfactory Memory Formation in Drosophila.” *Current Biology: CB* 22 (7): 608–14.
50. Kong, Eric C., Katherine Woo, Haiyan Li, Tim Lebestky, Nasima Mayer, Melissa R. Sniffen, Ulrike Heberlein, Roland J. Bainton, Jay Hirsh, and Fred W. Wolf. 2010. “A Pair of Dopamine Neurons Target the D1-like Dopamine Receptor DopR in the Central Complex to Promote Ethanol-Stimulated Locomotion in Drosophila.” *PloS One* 5 (4): e9954.
51. Kottler, Benjamin, Richard Faville, Jessika Cristina Bridi, and Frank Hirth. 2019. “Inverse Control of Turning Behavior by Dopamine D1 Receptor Signaling in Columnar and Ring Neurons of the Central Complex in Drosophila.” *Current Biology: CB* 29 (4): 567–77.e6.
52. Corfas, R. A., and M. H. Dickinson. 2018. “Diverse Food-Sensing Neurons Trigger Idiothetic Local Search in Drosophila.” *bioRxiv*. https://www.biorxiv.org/content/10.1101/433771v1.abstract.
53. Stone, Thomas, Barbara Webb, Andrea Adden, Nicolai Ben Weddig, Anna Honkanen, Rachel Templin, William Wcislo, Luca Scimeca, Eric Warrant, and Stanley Heinze. 2017. “An Anatomically Constrained Model for Path Integration in the Bee Brain.” *Current Biology: CB* 27 (20): 3069–85.e11.
54. Kakaria, Kyobi S., and Benjamin L. de Bivort. 2017. “Ring Attractor Dynamics Emerge from a Spiking Model of the Entire Protocerebral Bridge.” *Frontiers in Behavioral Neuroscience* 11 (February): 8.
55. Ormerod, Kiel G., Olivia K. LePine, Prabhodh S. Abbineni, Justin M. Bridgeman, Jens R. Coorssen, A. Joffre Mercier, and Glenn J. Tattersall. 2017. “Drosophila Development, Physiology, Behavior, and Lifespan Are Influenced by Altered Dietary Composition.” *Fly* 11 (3): 153–70.
56. Parnas, D., A. P. Haghighi, R. D. Fetter, S. W. Kim, and C. S. Goodman. 2001. “Regulation of Postsynaptic Structure and Protein Localization by the Rho-Type Guanine Nucleotide Exchange Factor dPix.” Neuron 32 (3): 415–24.
57. Lee, Tzumin, and Liqun Luo. 1999. “Mosaic Analysis with a Repressible Cell Marker for Studies of Gene Function in Neuronal Morphogenesis.” *Neuron*. https://doi.org/10.1016/s0896-6273(00)80701-1.
58. Yin, J. C., J. S. Wallach, M. Del Vecchio, E. L. Wilder, H. Zhou, W. G. Quinn, and T. Tully. 1994. “Induction of a Dominant Negative CREB Transgene Specifically Blocks Long-Term Memory in Drosophila.” *Cell* 79 (1): 49–58.
59. Brent, M. M., and I. I. Oster. 1974. “Nutritional Substitution: A New Approach to Microbial Control for Drosophila Cultures.” Drosophila Information Service 155: 157.
60. Budick, Seth A., and Michael H. Dickinson. 2006. “Free-Flight Responses of Drosophila Melanogaster to Attractive Odors.” *The Journal of Experimental Biology* 209 (Pt 15): 3001–17.

61. Honegger, Kyle S., Robert A. A. Campbell, and Glenn C. Turner. 2011. “Cellular-Resolution Population Imaging Reveals Robust Sparse Coding in the Drosophila Mushroom Body.” *The Journal of Neuroscience: The Official Journal of the Society for Neuroscience* 31 (33): 11772–85.
62. Hige, Toshihide, Yoshinori Aso, Mehrab N. Modi, Gerald M. Rubin, and Glenn C. Turner. 2015. “Heterosynaptic Plasticity Underlies Aversive Olfactory Learning in Drosophila.” *Neuron* 88 (5): 985–98.
63. Pologruto, Thomas A., Bernardo L. Sabatini, and Karel Svoboda. 2003. “ScanImage: Flexible Software for Operating Laser Scanning Microscopes.” *Biomedical Engineering Online* 2 (May): 13.
64. Grabe, Veit, Amelie Baschwitz, Hany K. M. Dweck, Sofia Lavista-Llanos, Bill S. Hansson, and Silke Sachse. 2016. “Elucidating the Neuronal Architecture of Olfactory Glomeruli in the Drosophila Antennal Lobe.” *Cell Reports* 16 (12): 3401–13.
65. R Core Team. 2019. “R: A Language and Environment for Statistical Computing.” *R Foundation for Statistical Computing.*
66. Nieuwenhuis, Sander, Birte U. Forstmann, and Eric-Jan Wagenmakers. 2011. “Erroneous Analyses of Interactions in Neuroscience: A Problem of Significance.” *Nature Neuroscience* 14 (9): 1105–7.
67.Stan Development Team. 2018. Stan User’s Guide Version 2.18. https://mc-stan.org/docs/2_18/stan-users-guide/index.html
68. Carpenter, Bob, Andrew Gelman, Matthew D. Hoffman, Daniel Lee, Ben Goodrich, Michael Betancourt, Marcus Brubaker, Jiqiang Guo, Peter Li, and Allen Riddell. 2017. “Stan: A Probabilistic Programming Language.” Journal of Statistical Software 76 (1). https://www.osti.gov/biblio/1430202.
69. Stan Development Team. 2018. RStan: the R interface to Stan. R package version 2.18.2. http://mc-stan.org/.
70. The No-U-turn sampler: adaptively setting path lengths in Hamiltonian Monte Carlo
71. Gabry, Jonah, Daniel Simpson, Aki Vehtari, Michael Betancourt, and Andrew Gelman. 2019. “Visualization in Bayesian Workflow.” *Journal of the Royal Statistical Society: Series A (Statistics in Society)* 182 (2): 389–402.

Supplementary Materials

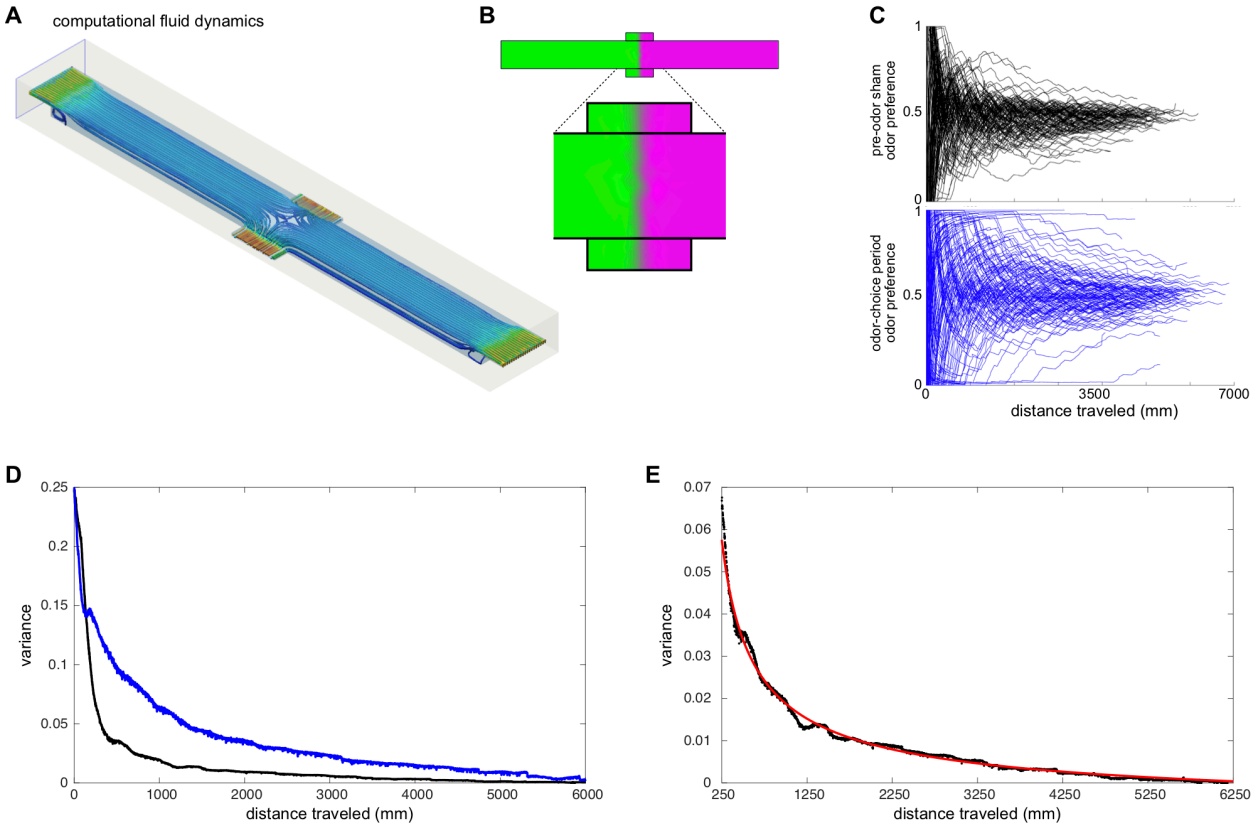
A
computational fluid dynamics
B
C
pre-odor sham
odor preference
odor-choice period
odor preference
1
0.5
0
0
3500
7000
distance traveled (mm)
D
variance
0.25
0.2
0.15
0.1
0.05
0
0
1000
2000
3000
4000
5000
6000
distance traveled (mm)
E
variance
0.07
0.06
0.05
0.04
0.03
0.02
0.01
0
250
1250
2250
3250
4250
5250
6250
distance traveled (mm)

Figure S1 — Dynamics of odor stimuli and behavioral variability

A) Computational Fluid Dynamics (CFD) simulation of steady state airflow through a single linear behavioral arena. Note the largely laminar flow along the length of the tunnel and the sharp flow boundary created in the center choice zone. Warmer colors indicate higher flow rates.

B) CFD scalar mixing simulation showing the distribution of odor concentration at steady state. The scenario simulated the flow of an odorized stream (magenta) in one end of the arena (outlined in black) and clean air (green) in the other. A steep gradient is observed in the center choice zone, with little diffusion into the opposite arm.

C) The running odor preference scores of 120 control (iso^{KH11}) flies as a function of distance traveled in the arena. Each line depicts the preference score trajectory of an individual fly. During the pre-odor period (top) most scores rapidly converge toward 0.5, but preference trajectories during the odor-choice period (bottom) are considerably more divergent.

D) Across-fly variance of the trajectories depicted in S1C as a function of distance traveled. During the pre-odor period (black) variance rapidly converges toward 0 as most flies approach a preference of 0.5, but during the odor-choice period (blue) across-fly variance stays much higher as flies exhibit preference for an odor.

E) Pre-odor period variance as a function of distance (black) fitted by the function var = 2.365 * $distance^{-0.651}$ - 0.0077 (red, R^2 = 0.96 for the region shown). This power-law relationship was used to calculate the activity-based variance offset for each fly.

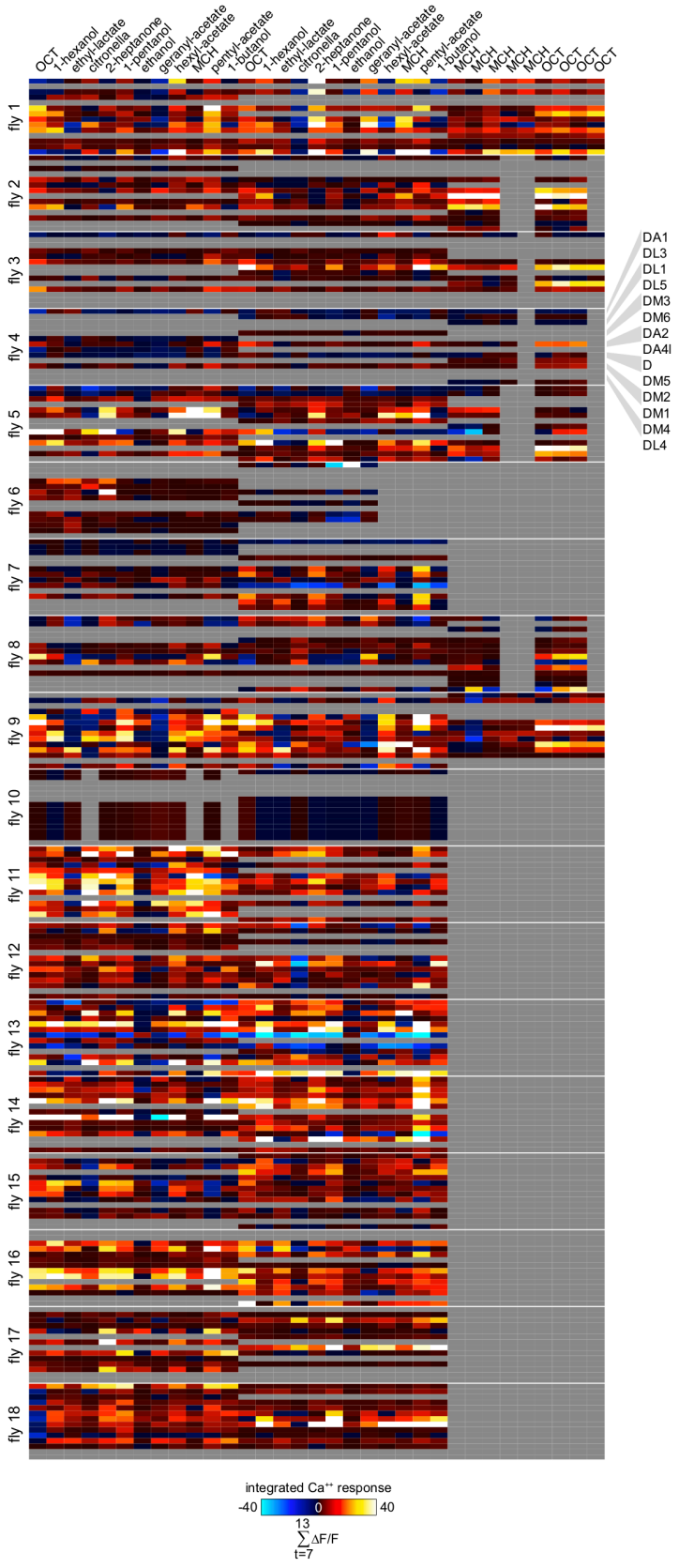
OCT
1-hexanol
ethyl-lactate
citronella
2-heptanone
1-pentanol
ethanol
geranyl-acetate
hexyl-acetate
MCH
pentyl-acetate
1-butanol
fly 1
fly 2
fly 3
fly 4
fly 5
fly 6
fly 7
fly 8
fly 9
fly 10
fly 11
fly 12
fly 13
fly 14
fly 15
fly 16
fly 17
fly 18
DA1
DL3
DL1
DL5
DM3
DM6
DA2
DA4l
D
DM5
DM2
DM1
DM4
DL4
integrated Ca++ response
-40
0
40
13
∑ ΔF/F
t=7

Figure S2 — Odor Ca^{++} response matrix for flies expressing GCaMP6m in GH146-Gal4 PNs. Integrated ΔF/F during and after the odor-stimulus period, by odor across the two 12 odor panels and OCT/MCH panel (columns). Rows are organized by individual fly and glomeruli.

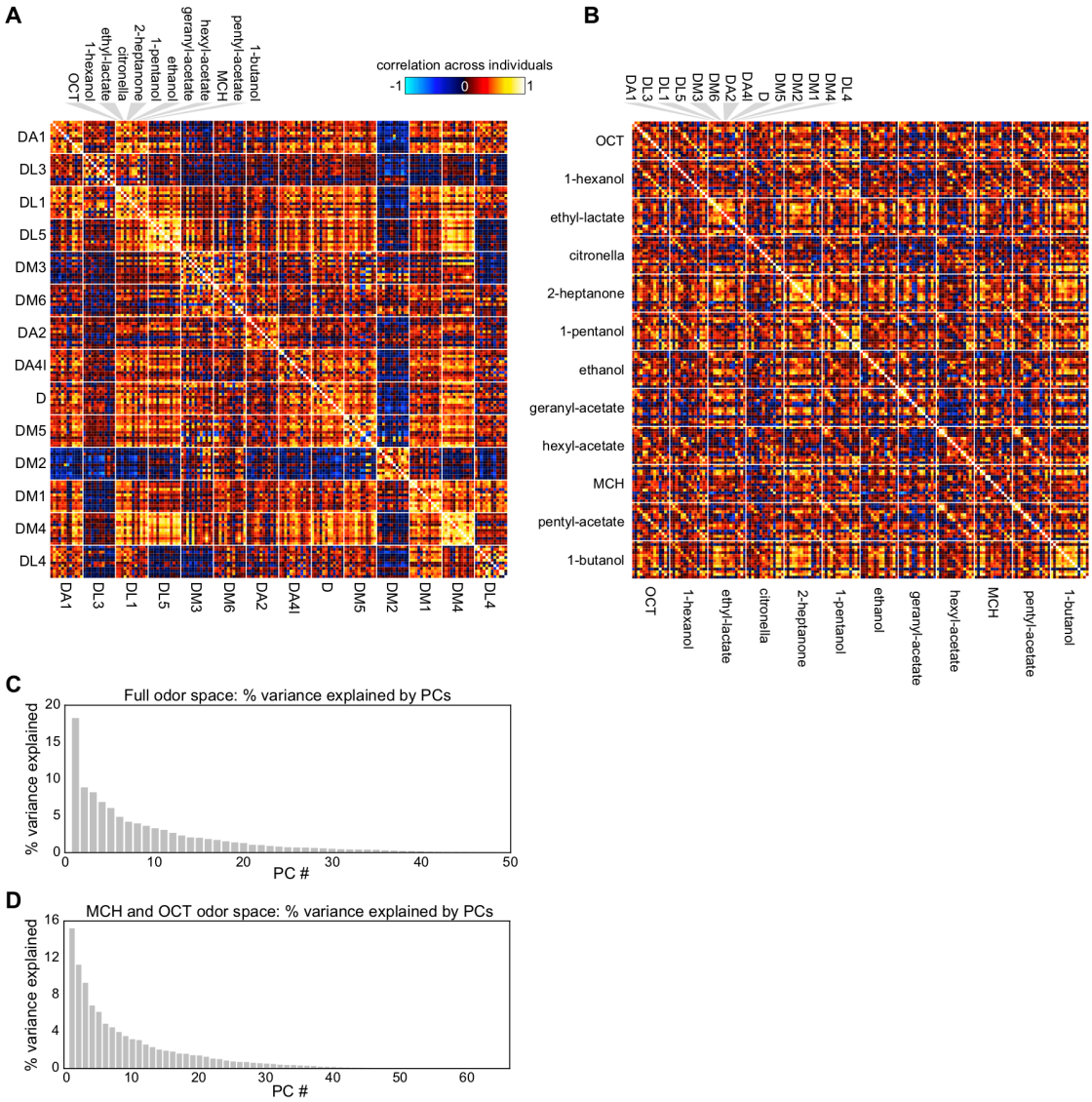
A
correlation across individuals
-1
0
1
OCT
1-hexanol
ethyl-lactate
citronella
2-heptanone
1-pentanol
ethanol
geranyl-acetate
hexyl-acetate
MCH
pentyl-acetate
1-butanol
DA1
DL3
DL1
DL5
DM3
DM6
DA2
DA4l
D
DM5
DM2
DM1
DM4
DL4
B
C
Full odor space: % variance explained by PCs
% variance explained
PC #
D
MCH and OCT odor space: % variance explained by PCs
% variance explained
PC #

Figure S3 — Structure of odor response covariance.

A) Correlation matrix of Ca^{++} responses across individual flies. Rows and columns are organized by glomerulus and then odor. Here all responses for each odor are averaged within each fly. I.e., OCT and MCH values reflect the average of up to nine values (two values from the 12 odor panels, and the remainder from the OCT/MCH trials). The values for all other odorants are the average of the two responses per fly in the 12 odor panels.

B) As in A), except rows and columns are organized by odor and then glomerulus.

C) Ranked eigenvalues of the principle components of a Ca^{++} response space in which individual 12 odor panel trials are points and glomerulus-odor pairs are dimensions (corresponding to Figure 2I).

D) As in C) except for a a Ca^{++} response space in which individual OCT or MCH trials are points and glomeruli are dimensions (corresponding to Figure 2J,K).

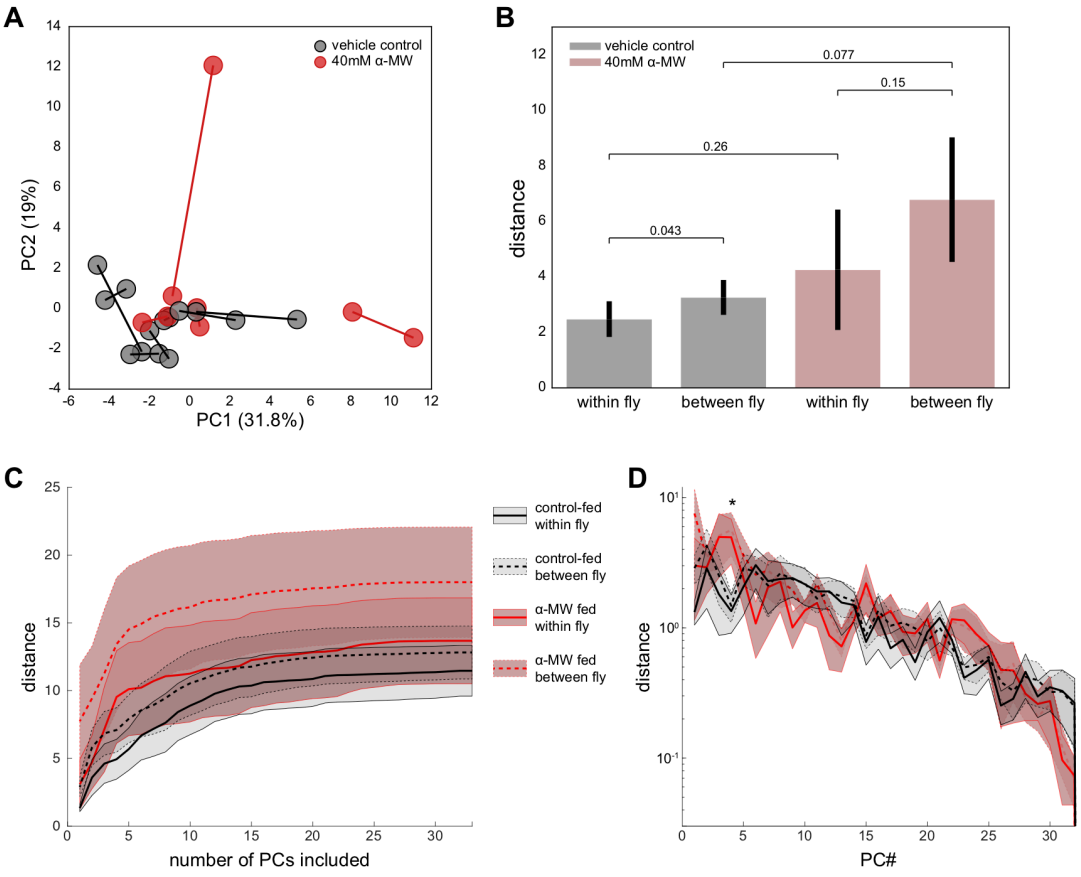
A
vehicle control
40mM α-MW
PC2 (19%)
PC1 (31.8%)
B
vehicle control
40mM α-MW
0.077
0.15
0.26
0.043
distance
within fly
between fly
within fly
between fly
C
control-fed within fly
control-fed between fly
α-MW fed within fly
α-MW fed between fly
distance
number of PCs included
D
*
distance
PC#

Figure S4 — Analysis of the robustness of the PCA results.

A) PCA embedding of 12 odor panel trials for a data set with no missing values, i.e., the largest complete data set that can be made from the values in Figure S7 (containing 6 control flies and 4 α-MW-fed flies, with responses to two 12 odor panels across four glomeruli each). Projection onto PC1 and PC2 of the two 12 odor panel responses. Lines connect paired panels for each individual.

B) Distance within and between flies in PC1-PC2 space for the data set used in A). Error bars are +/-1 standard error as determined by bootstrapping of individual flies. *P*-values within conditions reflect one-tailed resampling tests that the distance between flies is greater than the distance within. P-values between conditions reflect one-tailed resampling tests that α-MW distances are greater than control.

C) From the whole data set used in Figure 3E-G, distance between control-fed and α-MW-fed trials as a function of the dimensionality of the projected PC space in which distances are calculated. Shaded areas represent +/- standard error as calculated by bootstrap resampling.

D) As in C), but for distances (on a log y-axis) on just one PC at a time. α-MW-fed trials are significantly farther apart on PC4 than control trials (asterisk). $p = 0.028$ by bootstrapping based t-test comparing control and α-MW-fed inter-fly distances, and $p = 0.026$ for intra-fly distances.

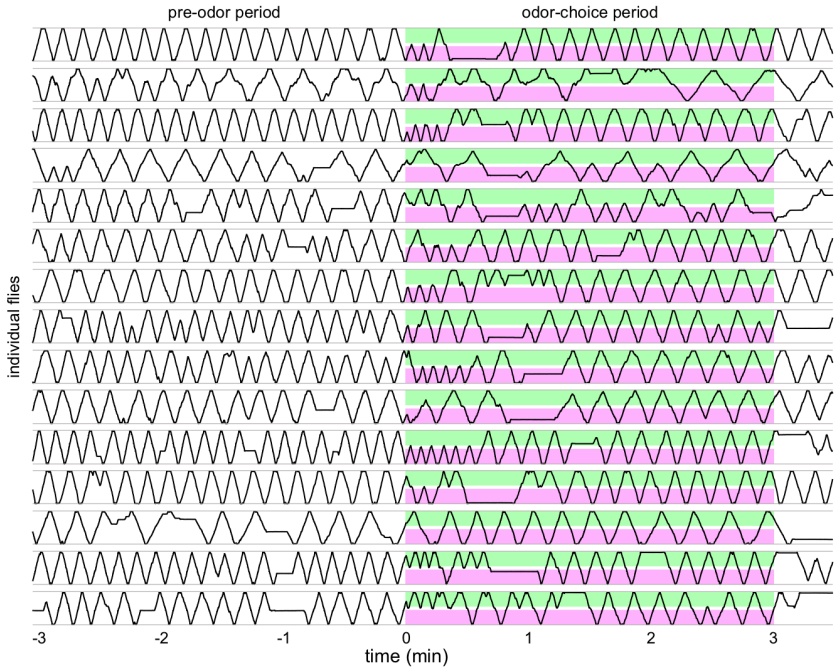
pre-odor period
odor-choice period
individual flies
-3
-2
-1
0
1
2
3
time (min)

Figure S5 — Sample individual kymographs of odor behavior for *Dop1R1* flies. Reversals (turning around at the odor boundary) during the odor-choice period, indicate that the flies are detecting the odorants. Magenta = OCT, green = MCH.

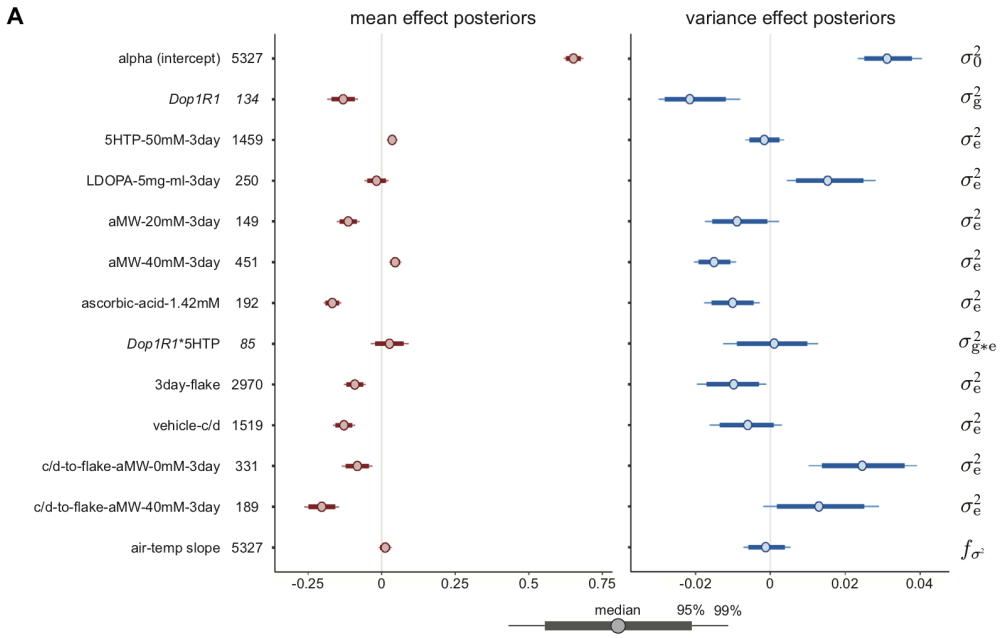
A
mean effect posteriors
variance effect posteriors
alpha (intercept) 5327
Dop1R1 134
5HTP-50mM-3day 1459
LDOPA-5mg-ml-3day 250
aMW-20mM-3day 149
aMW-40mM-3day 451
ascorbic-acid-1.42mM 192
Dop1R1*5HTP 85
3day-flake 2970
vehicle-c/d 1519
c/d-to-flake-aMW-0mM-3day 331
c/d-to-flake-aMW-40mM-3day 189
air-temp slope 5327
-0.25 0 0.25 0.5 0.75
-0.02 0 0.02 0.04
median 95% 99%

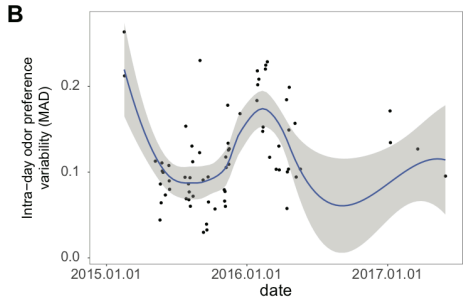
B
Intra−day odor preference variability (MAD)
0.0 0.1 0.2
2015.01.01 2016.01.01 2017.01.01
date

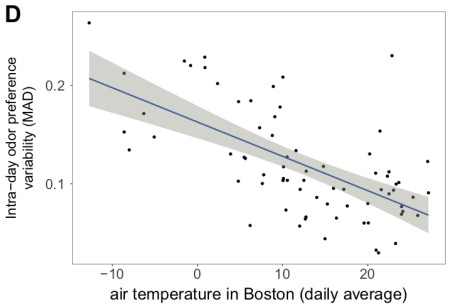
D
Intra−day odor preference variability (MAD)
0.1 0.2
−10 0 10 20
air temperature in Boston (daily average)

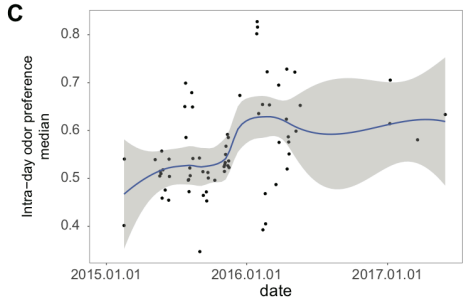
C
Intra−day odor preference median
0.4 0.5 0.6 0.7 0.8
2015.01.01 2016.01.01 2017.01.01
date

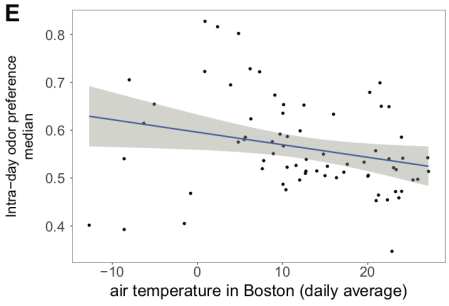
E
Intra−day odor preference median
0.4 0.5 0.6 0.7 0.8
−10 0 10 20
air temperature in Boston (daily average)

Figure S6 — Parameters of the Bayesian model of odor preference

A) Forest plot of the posterior distributions for all parameters of the neuromodulation and food-shock model (Figures 3C and 5B). Labels at right indicate which type of coefficient each parameter is in the term for variability (σ^2). Numbers by parameter labels at right indicate the "marginal sample size," i.e., the number of flies available to fit each parameter. c/d indicates cornmeal/dextrose media; flake indicates F4-24 food.

B) MAD (median absolute deviation) of wild type odor preferences measured daily (points) vs date. Blue line is a LOESS regression (span = 0.7), and grey region is the 95% CI. *n* = 3722.

C) As in B) for the daily median of odor preference.

D) MAD of wild type odor preferences measured daily (points) vs average daily temperature, as measured at the WBAN:14739 NOAA (Boston Logan International Airport) weather station. Blue line is a linear regression, and grey region is the 95% CI. *n* = 3722.

E) As in D) for the daily median of odor preference.

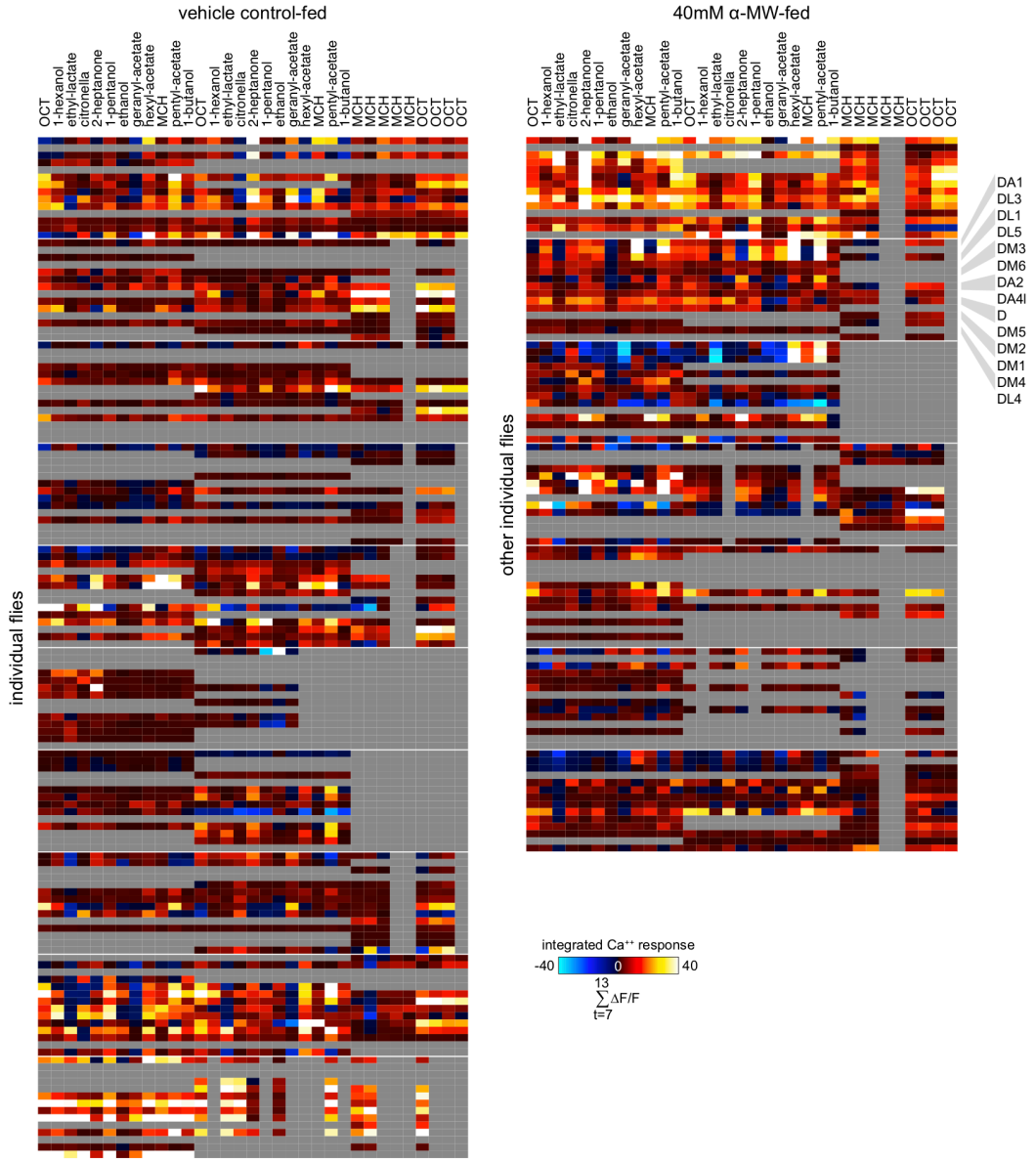
vehicle control-fed
40mM α-MW-fed
OCT
1-hexanol
ethyl-lactate
citronella
2-heptanone
1-pentanol
ethanol
geranyl-acetate
hexyl-acetate
MCH
pentyl-acetate
1-butanol
individual flies
other individual flies
DA1
DL3
DL1
DL5
DM3
DM6
DA2
DA4l
D
DM5
DM2
DM1
DM4
DL4
integrated Ca++ response
-40
0
40
13
∑ ΔF/F
t=7

Figure S7 — Odor Ca^{++} response matrices for control (left) and α-MW-fed (right) flies expressing GCaMP6m in GH146-Gal4 PNs. Integrated ΔF/F during and after the odor-stimulus period, by odor across the two 12 odor panels and OCT/MCH panel (columns). Rows are organized by individual fly and glomeruli.

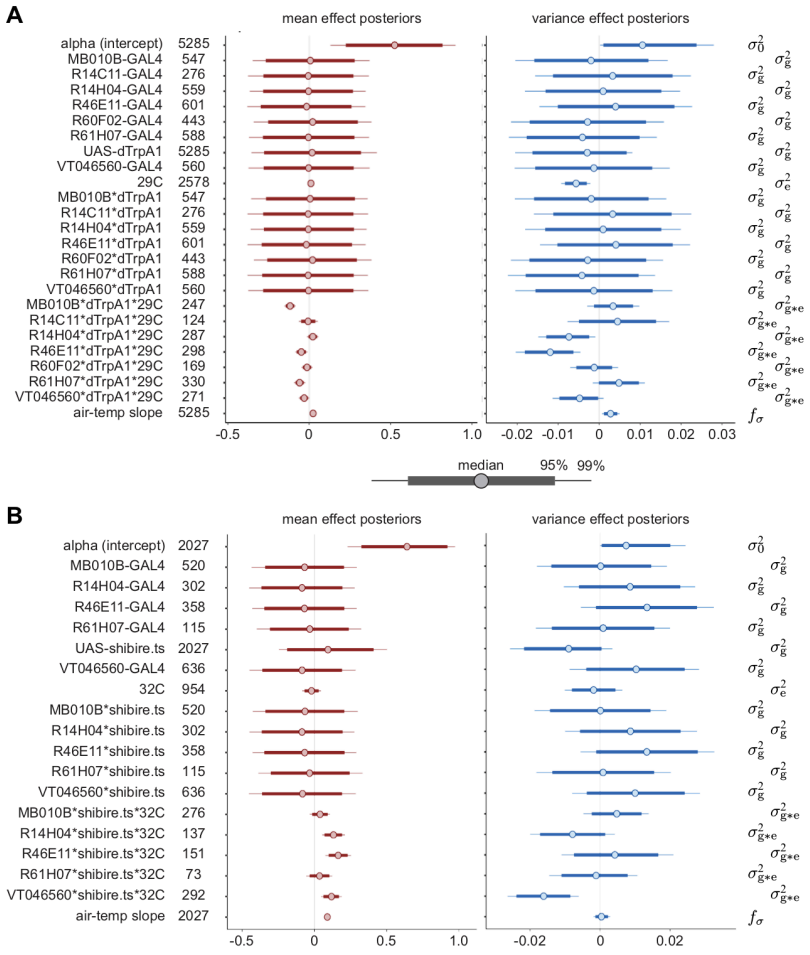
A
mean effect posteriors
variance effect posteriors
alpha (intercept) 5285
MB010B-GAL4 547
R14C11-GAL4 276
R14H04-GAL4 559
R46E11-GAL4 601
R60F02-GAL4 443
R61H07-GAL4 588
UAS-dTrpA1 5285
VT046560-GAL4 560
29C 2578
MB010B*dTrpA1 547
R14C11*dTrpA1 276
R14H04*dTrpA1 559
R46E11*dTrpA1 601
R60F02*dTrpA1 443
R61H07*dTrpA1 588
VT046560*dTrpA1 560
MB010B*dTrpA1*29C 247
R14C11*dTrpA1*29C 124
R14H04*dTrpA1*29C 287
R46E11*dTrpA1*29C 298
R60F02*dTrpA1*29C 169
R61H07*dTrpA1*29C 330
VT046560*dTrpA1*29C 271
air-temp slope 5285
-0.5 0 0.5 1.0
-0.02 -0.01 0 0.01 0.02 0.03
median
95%
99%
B
mean effect posteriors
variance effect posteriors
alpha (intercept) 2027
MB010B-GAL4 520
R14H04-GAL4 302
R46E11-GAL4 358
R61H07-GAL4 115
UAS-shibire.ts 2027
VT046560-GAL4 636
32C 954
MB010B*shibire.ts 520
R14H04*shibire.ts 302
R46E11*shibire.ts 358
R61H07*shibire.ts 115
VT046560*shibire.ts 636
MB010B*shibire.ts*32C 276
R14H04*shibire.ts*32C 137
R46E11*shibire.ts*32C 151
R61H07*shibire.ts*32C 73
VT046560*shibire.ts*32C 292
air-temp slope 2027
-0.5 0 0.5 1.0
-0.02 0 0.02

Figure S8 — Model parameters for thermogenetic experiments

A) Forest plot of the posterior distributions for all parameters of the neural circuit dTRPA1 activation model (Figure 4D). Labels at right indicate which type of coefficient each parameter is in the term for variability (σ^2). Numbers by parameter labels at right indicate the "marginal sample size," i.e., the number of flies available to fit each parameter.

B) As in A), for Shibire^{ts} experiments.